Flow of non-Newtonian fluids in single fractures and fracture networks: Current status, challenges, and knowledge gaps

Alexandre Lavrov [*]

Norwegian University of Science and Technology, Trondheim, Norway

A R T I C L E I N F O	A B S T R A C T
	Flow of non-Newtonian fluids in rock fractures is ubiquitous in engineering practice and involves e.g. cement flow in tunnel grouting, drilling fluid flow when a fracture is met during drilling, and flow of fracturing fluids in hydraulic fracturing. In this review article, basic information about rheological behavior of non-Newtonian fluids is provided in Section 1. In Section 2, a summary of equations for the flow of non-Newtonian fluids between smooth parallel plates is provided, and knowledge gaps are identified, including those in two-phase flow. In Section 3, non-Newtonian fluid flow in fracture networks is reviewed, and outstanding research tasks are identified. The article concludes with a summary of current challenges in Section 4. Amongst the main knowledge gaps and challenges identified in the review and relevant for engineering geological practice are fracture flow of thixotropic fluids; two-phase flow regimes and instabilities associated with it; flow of non-Newtonian fluids through (and their mixing with Newtonian fluids at) fracture intersections; efficient algorithms for network flow at arbitrary pressure gradients; leak-off of non-Newtonian fluids through fracture walls; modelling of non-Newtonian fluids that include environmental effects and the resulting multiple couplings and multiphysics.

1. Introduction: Non-Newtonian fluids

A non-Newtonian fluid is a fluid that has a nonlinear relationship between shear stress and shear rate in a simple shear flow. Non-Newtonian fluids are ubiquitous in everyday life and in industrial applications. Examples are ketchup, blood, cosmetics, toothpaste, foams, cement slurries, drilling fluids, some types of oil, hydraulic fracturing fluids, and partially crystallized magmas. In particular, in hydraulic fracturing, fluids with complex rheological properties are designed in order to satisfy multiple, often contradictory process requirements. For instance, creating a wide fracture requires high viscosity. On the other hand, preventing proppant settling to the bottom of the fracture necessitates rapid leak-off and fracture closure, which calls for lower fluid viscosity (Barbati et al., 2016). Drilling fluids present another example of complex non-Newtonian fluids often showing yield stress and memory about shearing history (Ren et al., 2021). Yield stress is required, in particular, in order to prevent settling of cuttings when the pumps are stopped. Non-Newtonian bentonite suspensions are used for seepage control in engineering geological applications [for instance, in order to prevent levee failures (Yoon and El Mohtar, 2014)].

Moreover, non-Newtonian rheology is exhibited by fluidized soil masses in flow-like landslides (Dai et al., 2014) and by some shales (Wüst and McLane, 2000). Examples from geological engineering where knowledge and understanding of non-Newtonian fluid flow in fractures are of paramount importance include grouting projects in underground construction, oil well stimulation jobs, and drilling of offshore wells. The importance of understanding the subsurface movement of non-Newtonian fluids in hazardous site remediation was realized already two decades ago (Hatheway and Reeves, 1999). Clays and clay-sand mixtures used to construct buffers (emplaced barriers) in radioactive-waste and spent-fuel disposal sites have non-Newtonian rheology that eventually determines their ability to hydrologically seal fractures (Baik et al., 2007; Grindrod et al., 1999). Our ability to predict the outcome of all these projects and to improve their design depends on our detailed information about how non-Newtonian fluids behave in different flow environments, both single-phase and multiphase.

The most commonly used models of non-Newtonian fluids belong to a subclass called generalized Newtonian fluids. For these fluids, the shear stress tensor, **S**, is related to the shear rate tensor, **D**, as follows (Irgens, 2008):

---

* Corresponding author.
  E-mail address: alexandre.lavrov@ntnu.no.

$$\mathbf{S} = 2\mu_a(\Gamma)\mathbf{D} \tag{1}$$

where Γ is the shear rate measure, given by $\Gamma = \sqrt{2\mathbf{D}:\mathbf{D}}$; μ_a is the apparent viscosity. For generalized Newtonian fluids, the apparent viscosity is thus only a function of the shear rate. Unlike a Newtonian fluid, for which the apparent viscosity is a constant (the dynamic viscosity), the apparent viscosity for a generalized Newtonian fluid is a function of the shear rate measure, and of that only. Only generalized Newtonian fluids will be discussed in this article. There are two reasons for this: (1) these are the models most frequently used in engineering geological applications (e.g. in hydraulic fracturing models) and (2) these are the models for which most of experimental and theoretical work has been done. For the sake of brevity, these will further be called non-Newtonian fluids here.

The behavior of non-Newtonian fluids can be illustrated by means of a unidirectional, simple shear flow (Fig. 1). Fig. 2 shows three examples of the shear stress vs. shear rate relationship ("flow curve") frequently used to describe the rheological behavior of non-Newtonian fluids. Amongst these models, Bingham fluid and Herschel-Bulkley fluids are yield-stress fluids: the shear stress must overcome a certain threshold level, the so-called yield stress, in order for the fluid to start flowing. Power-law fluid is an example of non-Newtonian fluid without yield stress.

For a power-law fluid, the apparent viscosity is given by (Irgens, 2008):

$$\mu_a = C\Gamma^{n-1} \tag{2}$$

where n is the flow index; C is the consistency index. For $n < 1$, the fluid is shear-thinning; for $n > 1$, the fluid is shear-thickening. In a simple shear flow (Fig. 1), the relationship between the shear stress, τ, and the shear rate, $\dot{\gamma}$, is thereby given by

$$\tau = C|\dot{\gamma}|^n \tag{3}$$

The power-law model is frequently employed to describe the rheological behavior of fluids (gels) used in hydraulic fracturing (Lakhtychkin et al., 2012; Perkowska et al., 2016). Magmas with a volume fraction of crystals from 25 to 40% to 50% exhibit power-law rheology (Lejeune and Richet, 1995; Ryerson et al., 1988).

Bingham fluid is defined as follows (Chin, 2012):

$$\mu_a = \mu_{pl} + \frac{\tau_Y}{\Gamma} \quad \text{if} \quad \sqrt{\frac{1}{2}\mathbf{S}:\mathbf{S}} > \tau_Y$$
$$\mathbf{D} = 0 \quad \text{if} \quad \sqrt{\frac{1}{2}\mathbf{S}:\mathbf{S}} < \tau_Y \tag{4}$$

The relationship between the shear stress and the shear rate in a simple shear flow is thereby given by

$$\tau = \tau_Y + \mu_{pl}|\dot{\gamma}| \tag{5}$$

where τ_Y is the yield stress; μ_{pl} is the plastic viscosity. The Bingham model is often employed to describe the rheology of drilling fluids (Caenn et al., 2011), cement grouts (Fidelibus and Lenti, 2012; Funehag and Thörn, 2018; Zou et al., 2018; Öge, 2017) and polymer gels used in improved oil recovery (Rossen and Kumar, 1992). Nonzero yield stress is
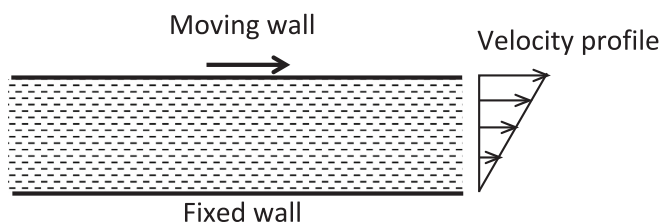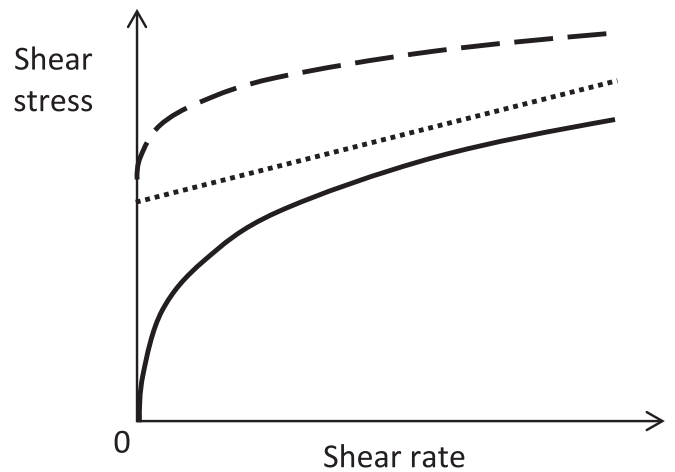

Fig. 2. Examples of non-Newtonian rheological models: power law with $n < 1$ (solid line), Bingham (dotted line) and Herschel-Bulkley with $n < 1$ (dashed line).

a required property of drilling fluids used to prevent settling of drill cuttings when the pumps are off. Magmas with a volume fraction of crystals in excess of 50% are known to have yield-stress rheology (Hallot et al., 1996).

Using the Bingham model in numerical calculations can be challenging since there is a discontinuity in the shear stress at $\dot{\gamma} = 0$. In order to facilitate the use of the Bingham rheology in numerical models, Eq. (4) is usually regularized, e.g. (Freitas et al., 2013; Frigaard and Nouar, 2005; Lavrov, 2005). Moreover, the concept of yield stress and the existence of a "true" yield stress have been debated in rheological literature for several decades (Barnes and Walters, 1985). Namely, finite yield stress implies infinite apparent viscosity at zero shear rate. Regularizations circumvent this issue by offering an approximation to the flow curve that has zero yield stress but otherwise closely follows the Bingham model.

Two types of regularization are particularly common: the bi-viscous model and the Papanastasiou regularization. In the bi-viscous model, the flow curve is piecewise linear (Fig. 3) (O'Donovan and Tanner, 1984). In the Papanastasiou regularization, the Bingham model is approximated with a smooth continuous function given by (Papanastasiou, 1987)

$$\mu_a = \mu_{pl} + \frac{\tau_Y[1 - exp(-m\Gamma)]}{\Gamma} \tag{6}$$

where m is a dimensionless regularization parameter. Increasing m brings the regularized stress-strain rate curve as closely to the Bingham
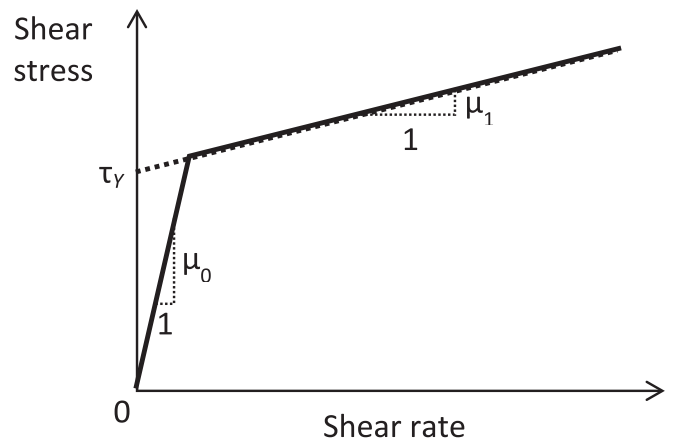

Fig. 3. *Bi-*viscous regularization (solid line) of the Bingham model (dotted line).

Fig. 1. Simple shear flow.

as necessary (Fig. 4).

Herschel-Bulkley fluid is defined as follows (Chin, 2012):

$$\mu_a = C\Gamma^{n-1} + \frac{\tau_Y}{\Gamma} \qquad \text{if} \quad \sqrt{\frac{1}{2}\mathbf{S}:\mathbf{S}} > \tau_Y$$

$$\mathbf{D} = 0 \qquad \qquad \text{if} \quad \sqrt{\frac{1}{2}\mathbf{S}:\mathbf{S}} < \tau_Y \tag{7}$$

The relationship between the shear stress and the shear rate in a simple shear flow is thereby given by

$$\tau = \tau_Y + C|\dot{\gamma}|^n \tag{8}$$

The Herschel-Bulkley model for a shear-thinning fluid ($n < 1$) is schematically shown in Fig. 2 (dashed line). The Herschel-Bulkley model is often employed to describe the rheology of drilling fluids (Cayeux, 2020; Majidi et al., 2008; Ofei et al., 2021; Russian et al., 2019) and cement grouts (Zou et al., 2020). In rock grouting applications, when a Herschel-Bulkley fluid is injected into a fracture system under a constant injection pressure, the yield stress controls the ultimate penetration distance while the consistency, C, affects the rate of the grout front propagation (Zou et al., 2020).

One of the issues with the Bingham model as well as with shear-thinning power-law and Herschel-Bulkley models is infinite apparent viscosity, $\tau/|\dot{\gamma}|$, at $|\dot{\gamma}| = 0$. To avoid this issue, the Carreau model can be used for shear-thinning fluids. The shear-thinning Carreau model ($n < 1$) is given by (Irgens, 2008)

$$\mu_a = \left\{ \mu_\infty + (\mu_0 - \mu_\infty)\left[1 + (\lambda\Gamma)^2\right]^{\frac{n-1}{2}} \right\} \tag{9}$$

where μ_0 is the viscosity at zero shear rate; μ_∞ is the limiting viscosity at $\dot{\gamma} \to \infty$; n and λ are fitting parameters.

A reasonable approximation of the Carreau model is provided by the truncated power-law model given by

$$\mu_a = \begin{cases} \mu_0, & \text{if} \quad \Gamma < \dot{\gamma}_1 \\ C\Gamma^{n-1} & \text{if} \quad \dot{\gamma}_1 < \Gamma < \dot{\gamma}_2 \\ \mu_\infty & \text{if} \quad \Gamma > \dot{\gamma}_2 \end{cases} \tag{10}$$

where $\dot{\gamma}_1 = (C/\mu_0)^{1/(1-n)}$ and $\dot{\gamma}_2 = (C/\mu_\infty)^{1/(1-n)}$ represent cut-off values of the shear rate. At $\Gamma < \dot{\gamma}_1$, the truncated power-law fluid behaves like a Newtonian fluid with viscosity μ_0. At $\Gamma > \dot{\gamma}_2$, the truncated power-law fluid behaves like a Newtonian fluid with viscosity μ_∞. At intermediate shear rates, $\dot{\gamma}_1 < \Gamma < \dot{\gamma}_2$, the truncated power-law fluid behaves like a power-law fluid. Truncated power-law rheology has been employed to model hydraulic fracturing (Wrobel et al., 2021).

To illustrate the values of the parameters used to describe non-Newtonian fluids, a few examples are provided in Table 1.
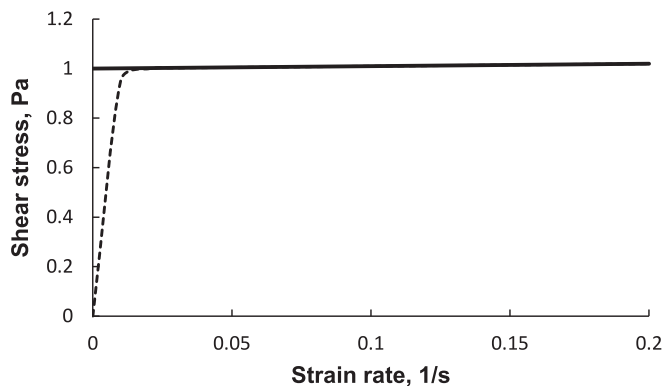
Table 1
Examples of measured parameters for different rheological models.

Fluid	Model	Parameters	Reference
Portland cement grout	Power law	$C = 1.4278$ Pa•s$^{0.616}$, $n = 0.616$	(Liu et al., 2018)
Portland cement grout	Bingham	$\tau_Y = 3.032$ Pa, $\mu_{pl} = 0.018$ Pa•s	(Liu et al., 2018)
Oil-based drilling fluid	Herschel-Bulkley	$\tau_Y = 1.73$ Pa, $C = 0.062$ Pa•s$^{0.876}$, $n = 0.876$	(Sayindla et al., 2019)
KCl/polymer (xanthan gum) water-based drilling fluid	Herschel-Bulkley	$\tau_Y = 2.23$ Pa, $C = 1.009$ Pa•s$^{0.379}$, $n = 0.379$	(Cayeux and Leulseged, 2019)

It should be remembered that properties of non-Newtonian fluids depend on the environmental conditions, in particular temperature (Cayeux, 2020; Metwally et al., 2022) and salinity (Ren et al., 2021). This may become important, for instance, when injecting these fluids into rock masses that have elevated temperature. Adding solid particles (e.g. lost-circulation materials) to a non-Newtonian fluid alters its rheological properties, too.

In addition to nonlinear flow curves, some non-Newtonian fluids demonstrate thixotropic behavior: their rheological properties depend on the shear history experienced by the fluid. Shearing may either destroy the network structures of particles in the fluid (positive thixotropy) or build up a new particle arrangement due to particle aggregation (negative thixotropy). The former scenario reduces the fluid viscosity; the latter increases it (Ren et al., 2021). Thixotropy introduces a wide spectrum of additional complications in the fluid behavior. For instance, cyclic increase-decrease of the shear rate results in a hysteresis of the flow curve. An example for a fluid with positive thixotropy is schematically shown in Fig. 5. Discussion of time-dependent effects in geological applications is continued in Section 2.

The behavior of non-Newtonian fluids is by far more diverse than what a brief overview can cover. For instance, some fluids used in hydraulic fracturing may show viscoelastic behavior, normal stress differences, extensional viscosity, material memory, strain dependence etc. (Barbati et al., 2016). In this paper, I choose to focus on generalized non-Newtonian fluids (for which shear stress only depends on the shear rate) as the most common non-Newtonian fluids used in engineering geological applications.

The focus of this review article is on fracture flow of non-Newtonian fluids. Fracture flow of Newtonian fluids is not covered in this article.
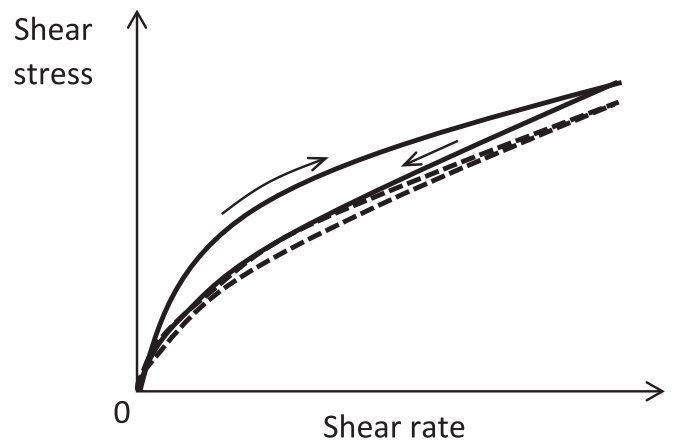

Fig. 4. Example of the Papanastasiou regularization (dashed line) of the Bingham model (solid line). $\tau_Y = 1$ Pa, $\mu_{pl} = 0.1$ Pa•s, m = 300.

Fig. 5. Flow curve for a thixotropic fluid subjected to cyclic increase/decrease in the share rate. Solid line: first cycle; dashed line: second cycle. Based on (Billingham and Ferguson, 1993).

Comprehensive research has been conducted on Newtonian fluid flow in fractures and fracture networks over the past three decades. This research is covered in numerous publications starting from e.g. (Brown, 1987) and onwards.

2. Flow of non-Newtonian fluids in a single fracture

2.1. Single-phase flow between smooth parallel walls

Real fractures have rough walls. However, in numerical models, fractures are often assumed to be smooth, with the distance between the fracture faces being equal to the so-called hydraulic aperture of the fracture (Selvadurai and Nguyen, 1999). Hydraulic aperture is defined as the aperture of a smooth-walled fracture that, under a given pressure difference, produces the same flow rate as the real rough-walled fracture (Békri et al., 1997; Brown, 1987). For the above reason, we begin our exposition of fracture flow with single-phase flow between two smooth parallel walls.

Laminar flow of a Newtonian fluid in a smooth-walled conduit of constant aperture w is described by the so-called "cubic law". According to this law, the average fluid velocity, v, in a one-dimensional fracture is given by

$$v = -\frac{w^2}{12\mu}\frac{dP}{dx} \tag{11}$$

where x is directed along the fracture; P is the fluid pressure; μ is the dynamic viscosity of the fluid. Eq. (11) is used e.g. to describe the Newtonian fluid flow in two-dimensional discrete fracture networks (DFNs) where each fracture is represented by a line segment (Fig. 6). "Average fluid velocity" here means that the fluid velocity is averaged across the aperture. Flow rate per unit length in the direction normal to the drawing in Fig. 6 is given by the product of v and w and is thus proportional to w^3; thus, the name "cubic law".

In a planar, two-dimensional fracture located in plane x, y, the vector of average fluid velocity is given by

$$\mathbf{v} = -\frac{w^2}{12\mu}\nabla P = -\frac{w^2}{12\mu}\left(\frac{\partial P}{\partial x}, \frac{\partial P}{\partial y}\right) \tag{12}$$
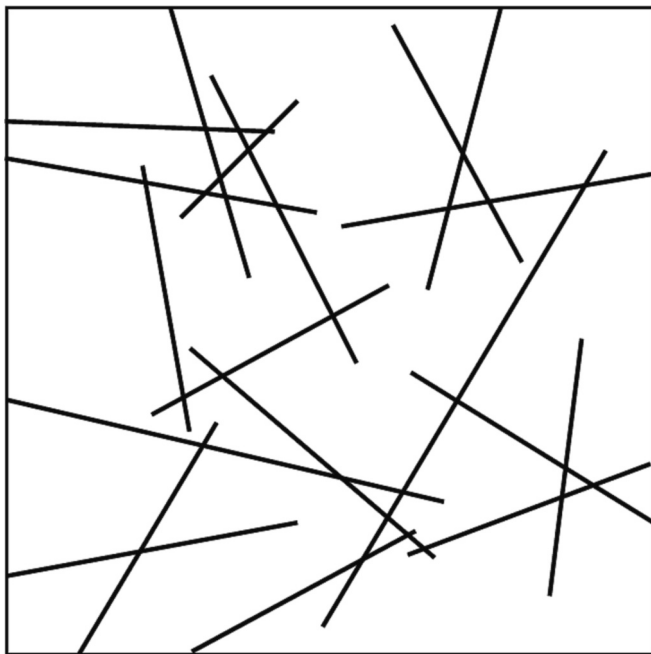

Fig. 6. Two-dimensional discrete fracture network (DFN) consisting of one-dimensional, linear fractures.

where ∇P is the pressure gradient in the fracture plane.

Eq. (12) and similar equations for non-Newtonian fluids quoted later in this Section are obtained by solving the momentum conservation equation for laminar flow, with the shear rate tensor given by

$$\mathbf{D} = \begin{bmatrix} 0 & 0 & \frac{1}{2}\frac{\partial u_x}{\partial z} \\ 0 & 0 & \frac{1}{2}\frac{\partial u_y}{\partial z} \\ \frac{1}{2}\frac{\partial u_x}{\partial z} & \frac{1}{2}\frac{\partial u_y}{\partial z} & 0 \end{bmatrix} \tag{13}$$

the shear stress tensor given by

$$\mathbf{S} = \begin{bmatrix} 0 & 0 & \tau_{xz} \\ 0 & 0 & \tau_{yz} \\ \tau_{xz} & \tau_{yz} & 0 \end{bmatrix}, \tag{14}$$

and the constitutive law given by Eq. (1).

2.1.1. Power-law fluid

For non-Newtonian fluids, closed-form solutions for the average fluid velocity can be obtained for only few rheological models. In particular, for a power-law fluid flowing in a 1D, linear fracture (Chhabra and Richardson, 1999):

$$v = -\frac{n}{2n+1}\frac{1}{C^{1/n}}\left(\frac{w}{2}\right)^{(n+1)/n}\left|\frac{dP}{dx}\right|^{(1-n)/n}\frac{dP}{dx} \tag{15}$$

For a Newtonian fluid, Eq. (15) becomes Eq. (11) if we substitute $C = \mu$, $n = 1$.

For a power-law fluid flowing in a 2D, planar fracture, the vector of average velocity is given by

$$\mathbf{v} = -\frac{n}{2n+1}\frac{1}{C^{1/n}}\left(\frac{w}{2}\right)^{(n+1)/n}|\nabla P|^{(1-n)/n}\nabla P \tag{16}$$

For a Newtonian fluid, Eq. (16) becomes Eq. (12) if we substitute $C = \mu$, $n = 1$.

2.1.2. Bingham fluid

For a Bingham fluid flowing in a linear, 1D fracture the average fluid velocity is given by

$$v = \begin{cases} 0 & \text{if } \left|\frac{dP}{dx}\right| < \frac{2\tau_Y}{w} \\ \left(-\frac{w^2}{12\mu_{pl}} + \frac{1}{4}\frac{w\tau_Y}{\mu_{pl}|dP/dx|} - \frac{1}{3}\frac{\tau_Y^3}{\mu_{pl}w|dP/dx|^3}\right)\frac{dP}{dx} & \text{if } \left|\frac{dP}{dx}\right| > \frac{2\tau_Y}{w} \end{cases} \tag{17}$$

Eq. (17) becomes Eq. (11) if we substitute $\mu_{pl} = \mu$, $\tau_Y = 0$ (Newtonian fluid).

For a Bingham fluid flowing in a 2D planar fracture, the vector of average velocity is given by

$$\mathbf{v} = \begin{cases} 0 & \text{if } |\nabla P| < \frac{2\tau_Y}{w} \\ \left(-\frac{w^2}{12\mu_{pl}} + \frac{1}{4}\frac{w\tau_Y}{\mu_{pl}|\nabla P|} - \frac{1}{3}\frac{\tau_Y^3}{\mu_{pl}w|\nabla P|^3}\right)\nabla P & \text{if } |\nabla P| > \frac{2\tau_Y}{w} \end{cases} \tag{18}$$

If $w|\nabla P|/\tau_Y \gg 1$, the last term in the parentheses on the right-hand side of Eq. (18$_2$) is negligible compared to the first two terms. Neglecting the last term then leads to a linearized form of this equation that was employed e.g. in (Liu et al., 2021).

When Bingham fluid flows in a fracture of constant aperture, a solid core exists in the region of low shear rate, i.e. around the mid-plane of the fracture (the xy-plane located at an equal distance from the fracture

faces) (Amadei and Savage, 2001). The thickness of this solid, unyielded core is given by $2\tau_Y/|\nabla P|$. Eqs. (17) and (18) imply that there is no flow when the pressure gradient is below a critical value, $2\tau_Y/w$. Under this condition, the solid core occupies the entire fracture aperture, and the flow stops (the fluid becomes immobile, $\mathbf{v} = 0$). This usually creates convergence problems when Eq. (18) is used to model fracture flow of a Bingham fluid numerically. In order to circumvent this problem, regularized Bingham models are used. The Papanastasiou regularization discussed in Section 1 prevents the formation of solid core and thus of immobile fluid regions. It turns out, however, that a closed-form solution for the fluid velocity as a function of pressure gradient requires in this case solving a transcendental differential equation, and thus cannot be obtained. Nevertheless, there are at least two ways how closed-form solutions approximating the Bingham fluid flow in a fracture can be obtained. The first one is the use of bi-viscous regularization (Section 1). This results in a closed-form solution for the average fluid velocity (Lenci and Di Federico, 2020):

$$v = \begin{cases} -\dfrac{w^2}{12\mu_0}\dfrac{dP}{dx} & \text{if } \left|\dfrac{dP}{dx}\right| < \dfrac{2\tau_Y\mu_0}{w(\mu_0-\mu_1)} \\[3mm] \left(-\dfrac{w^2}{12\mu_1} - \dfrac{\tau_Y^3\mu_0^2}{3w\mu_1(\mu_0-\mu_1)^2|dP/dx|^3} + \dfrac{\tau_Y w}{4\mu_1|dP/dx|}\right)\dfrac{dP}{dx} & \text{if } \left|\dfrac{dP}{dx}\right| > \dfrac{2\tau_Y\mu_0}{w(\mu_0-\mu_1)} \end{cases} \tag{19}$$

where μ_0 is the slope of the flow curve at low shear rates, i.e. at shear rates below $\tau_Y/(\mu_0-\mu_1)$; μ_1 is the slope of the flow curve at high shear rates, i.e. at shear rates above $\tau_Y/(\mu_0-\mu_1)$ (Fig. 3); $\mu_0 > \mu_1$. A different arrangement of Eq. (19) is provided in (Lavrov, 2005).

For a bi-viscous fluid flowing in a 2D planar fracture, the vector of average velocity is given by:

$$\mathbf{v} = \begin{cases} -\dfrac{w^2}{12\mu_0}\nabla P & \text{if } |\nabla P| < \dfrac{2\tau_Y\mu_0}{w(\mu_0-\mu_1)} \\[3mm] \left(-\dfrac{w^2}{12\mu_1} - \dfrac{\tau_Y^3\mu_0^2}{3w\mu_1(\mu_0-\mu_1)^2|\nabla P|^3} + \dfrac{\tau_Y w}{4\mu_1|\nabla P|}\right)\nabla P & \text{if } |\nabla P| > \dfrac{2\tau_Y\mu_0}{w(\mu_0-\mu_1)} \end{cases} \tag{20}$$

Another regularization for Bingham fluid flow in fractures, the "SINTEF model", was developed in (Bao et al., 2017). It was obtained by regularizing directly Eqs. (17) and (18) rather than the Bingham model, i.e. Eqs. (4)–(5). This approach results in the following equation for 1D fracture flow:

$$v = -\frac{w\tau_Y}{\mu_{pl}|dP/dx|}\frac{dP}{dx}\left\{\left[\left(\frac{1}{4}\right)^\lambda + \left(\frac{|dP/dx|w}{12\tau_Y}\right)^\lambda\right]^{1/\lambda} - \frac{1}{4}\right\} \quad \text{for all } dP/dx. \tag{21}$$

where λ is a dimensionless regularization parameter. In 2D fractures the following equation can be used:

$$\mathbf{v} = -\frac{w\tau_Y}{\mu_{pl}}\left\{\left[\left(\frac{1}{4}\right)^\lambda + \left(\frac{|\nabla P|w}{12\tau_Y}\right)^\lambda\right]^{1/\lambda} - \frac{1}{4}\right\}\frac{\nabla P}{|\nabla P|} \quad \text{for all } |\nabla P|. \tag{22}$$

From numerical viewpoint, an important advantage of Eq. (21) compared to both the Bingham model Eq. (17) and the bi-viscous regularized model Eq. (19) is that it is valid for *all* values of the pressure gradient. However, at small pressure gradients, Eq. (21) involves subtraction of two close numbers. This is known to increase the computational error (Ralston and Rabinowitz, 2016). As shown in (Bao et al., 2017), Taylor expansion of the right-hand side of Eq. (21) yields the following approximation of Eq. (21):

$$v \approx -\frac{1}{4\lambda}\left(\frac{|dP/dx|w}{3\tau_Y}\right)^\lambda\frac{dP/dx}{|dP/dx|} \quad \text{for } \frac{|dP/dx|w}{2\tau_Y} << 1 \tag{23}$$

and similarly for 2D flow:

$$\mathbf{v} \approx -\frac{1}{4\lambda}\left(\frac{|\nabla P|w}{3\tau_Y}\right)^\lambda\frac{\nabla P}{|\nabla P|} \quad \text{for } \frac{|\nabla P|w}{2\tau_Y} << 1 \tag{24}$$

Accuracy of approximations with regularized models depends on the regularization parameters, i.e. the ratio μ_0/μ_1 in Eq. (19) and λ in Eq. (21). This is illustrated in Fig. 7a where three 1D flow models are plotted for a fracture of aperture $w = 1$ mm: Bingham model [Eq. (17)], bi-viscous model [Eq. (19)] and SINTEF model [Eq. (21)]. The following values were used in the Bingham model: $\tau_Y = 10$ Pa, $\mu_{pl} = 0.01$ Pa•s. In the bi-viscous model, $\mu_1 = \mu_{pl}$ and $\mu_0/\mu_1 = 10$. In the SINTEF model, $\lambda = 4$. The approximations are quite good at higher pressure gradient values and become somewhat worse at lower pressure gradients.

According to (Lenci and Di Federico, 2020), bi-viscous model provides a good approximation of the Bingham model when $\mu_0/\mu_1 = 100...1000$. When bi-viscous model is used in flow simulations with rough-walled fractures, the accuracy of approximation decreases with the roughness and improves with the pressure gradient (Lenci and Di Federico, 2020).

Accuracy of approximation at lower pressure gradients is improved in Fig. 7b by changing the regularization parameters to $\mu_0/\mu_1 = 100$ in the bi-viscous model and $\lambda = 6$ in the SINTEF model. The rest of the parameters are the same as in Fig. 7a.

2.1.3. Herschel-Bulkley fluid

For a Herschel-Bulkley fluid flowing in a linear, 1D fracture the average fluid velocity is given by (Morris et al., 2015)

$$v = \begin{cases} 0 & \text{if } \left|\dfrac{dP}{dx}\right| < \dfrac{2\tau_Y}{w} \\[3mm] \dfrac{2n}{n+1}\dfrac{1}{C^{1/n}w|dP/dx|^2}\dfrac{dP}{dx}\left[\dfrac{n}{2n+1}\dfrac{1}{|dP/dx|}\left(\dfrac{w|dP/dx|}{2}-\tau_Y\right)^{(2n+1)/n} - \dfrac{w}{2}\left(\dfrac{w|dP/dx|}{2}-\tau_Y\right)^{(n+1)/n}\right] & \text{if } \left|\dfrac{dP}{dx}\right| > \dfrac{2\tau_Y}{w} \end{cases} \tag{25}$$
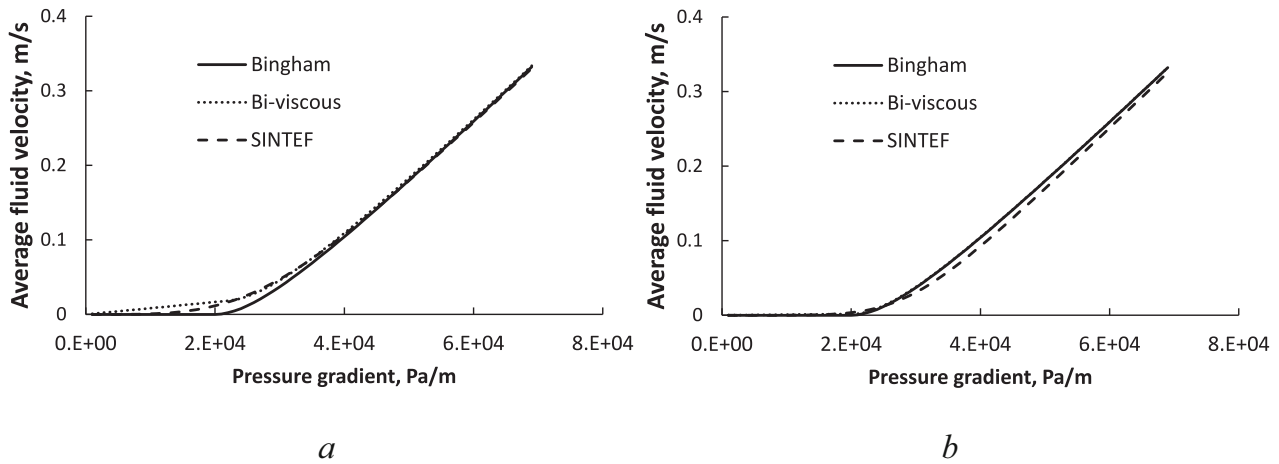
Fig. 7. Bingham model (solid line), bi-viscous model (dotted line) and SINTEF model (dashed line) obtained with the following regularization parameters:
(a) $\mu_0/\mu_1 = 10$ in the bi-viscous model, $\lambda = 4$ in the SINTEF model.
(b) $\mu_0/\mu_1 = 100$ in the bi-viscous model, $\lambda = 6$ in the SINTEF model.
The rest of parameters are quoted in the bulk text.

Eq. (25) becomes Eq. (17) for $n = 1.0$ (Bingham fluid).

For a Herschel-Bulkley fluid flowing in a 2D planar fracture, the vector of average velocity is given by

$$
\mathbf{v} = \begin{cases} 0 & \text{if } |\nabla P| \langle \frac{2\tau_Y}{w} \\ \frac{2n}{n+1} \frac{\nabla P}{C^{1/n} w |\nabla P|^2} \left[\frac{n}{2n+1} \frac{1}{|\nabla P|} \left(\frac{w|\nabla P|}{2} - \tau_Y \right)^{(2n+1)/n} - \frac{w}{2} \left(\frac{w|\nabla P|}{2} - \tau_Y \right)^{(n+1)/n} \right] & \text{if } |\nabla P| \rangle \frac{2\tau_Y}{w} \end{cases} \tag{26}
$$

2.1.4. Truncated power-law fluid

For a truncated power-law fluid flowing in a linear, 1D fracture the average fluid velocity is given by (Lavrov, 2015; Wrobel, 2020)

$$
v = \begin{cases} -\frac{w^2}{12\mu_0} \frac{dP}{dx} & \text{if } \left| \frac{dP}{dx} \right| \langle \frac{2\mu_0 \dot{\gamma}_1}{w} \\ \left[-\frac{2}{3} \frac{1-n}{1+2n} \frac{C^{3/(1-n)}}{w\mu_0^{(1+2n)/(1-n)} |dP/dx|^3} - \frac{2n}{1+2n} \frac{(w/2)^{(1+2n)/n}}{wC^{1/n}} \left| \frac{dP}{dx} \right|^{(1-n)/n} \right] \frac{dP}{dx} & \text{if } \frac{2\mu_0 \dot{\gamma}_1}{w} < \left| \frac{dP}{dx} \right| \langle \frac{2C\dot{\gamma}_2^n}{w} \\ \left\{ -\frac{w^2}{12\mu_0} + \frac{2}{3} \frac{1-n}{1+2n} \frac{C^{3/(1-n)}}{w|dP/dx|^3} \left[\frac{1}{\mu_\infty^{(1+2n)/(1-n)}} - \frac{1}{\mu_0^{(1+2n)/(1-n)}} \right] \right\} \frac{dP}{dx} & \text{if } \left| \frac{dP}{dx} \right| \rangle \frac{2C\dot{\gamma}_2^n}{w} \end{cases} \tag{27}
$$

For a truncated power-law fluid flowing in a 2D planar fracture, the vector of average velocity is given by:

$$
\mathbf{v} = \begin{cases} -\frac{w^2}{12\mu_0} \nabla P & \text{if } |\nabla P| \langle \frac{2\mu_0 \dot{\gamma}_1}{w} \\ \left[-\frac{2}{3} \frac{1-n}{1+2n} \frac{C^{3/(1-n)}}{w\mu_0^{(1+2n)/(1-n)} |dP/dx|^3} - \frac{2n}{1+2n} \frac{(w/2)^{(1+2n)/n}}{wC^{1/n}} \left| \frac{dP}{dx} \right|^{(1-n)/n} \right] \nabla P & \text{if } \frac{2\mu_0 \dot{\gamma}_1}{w} < |\nabla P| \langle \frac{2C\dot{\gamma}_2^n}{w} \\ \left\{ -\frac{w^2}{12\mu_0} + \frac{2}{3} \frac{1-n}{1+2n} \frac{C^{3/(1-n)}}{w|dP/dx|^3} \left[\frac{1}{\mu_\infty^{(1+2n)/(1-n)}} - \frac{1}{\mu_0^{(1+2n)/(1-n)}} \right] \right\} \nabla P & \text{if } |\nabla P| \rangle \frac{2C\dot{\gamma}_2^n}{w} \end{cases} \tag{28}
$$

As pointed out in (Rodríguez de Castro and Radilla, 2017), truncated power-law model is not adequate for fracture flow of real complex shear-thinning fluids when shear rates reach transition from the power-law range to the upper Newtonian plateau.

2.1.5. Other models

Exact closed-form solutions for flow between parallel walls exist only for a limited number of rheological models. A novel method of deriving an approximate relation between pressure gradient and flow rate for a smooth-walled fracture, for *any* generalized Newtonian rheology, was proposed in (Wrobel, 2020). According to this method, first, a piecewise approximation of the apparent viscosity is made in different shear rate intervals. This approximation is continuous and is achieved with power-law functions. The resulting approximate flow curve can be viewed as a generalization of truncated power-law model, with several power-law intervals instead of just one, as in Eq. (10). The approximation can be made as accurate as desired by increasing the number of power-law intervals. It turns out that such piecewise-power-law fluid allows an analytical, closed-form solution for the flow rate (or average velocity) vs. pressure gradient in a smooth-walled fracture. Thus, the average velocity can be analytically computed for any type of generalized Newtonian rheology, with any required accuracy.

The above-discussed rheological models are generalized Newtonian models. Thus, none of them take time-dependent properties into account. One example of time-dependency is thixotropy. Thixotropy is known e.g. in drilling fluids (Cayeux, 2020). Experiments show that shear history may affect the behavior of thixotropic fluids over long transport distances. For instance, when a drilling fluid or cement enter a fracture intersected by the borehole, the shear rate undergoes a sudden change. The effect of such a change on fracture flow of a thixotropic fluid has apparently never been properly investigated (theoretically or experimentally). Since performing such an experiment might be quite challenging, a first step could be a numerical model. Building such a numerical model is, however, a challenge, too, since thixotropic models that could describe the real behavior of e.g. drilling fluids contain many parameters; for instance, the thixotropic model developed in (Cayeux, 2020) has 18 parameters (instead of just three for a non-thixotropic Herschel-Bulkley fluid). In addition, using such models in fluid dynamics simulations of fracture flow would necessitate tracing the shear history of individual fluid volumes — a task formidable indeed, also in terms of computational time.

Thixotropic properties may be particularly relevant when fluid flow is cyclic, for instance, during the so-called borehole ballooning events in drilling (Lavrov and Tronvoll, 2005). During ballooning, the drilling fluid flows into and out of a fracture in cycles due to the variations in the downhole pressure. The fluid movement into and out of the fracture is due to the opening/closing of the fracture, without the fracture necessarily propagating further into the formation. Thixotropic effects are likely to influence especially the beginning phase of each inflow or outflow cycle.

Another example of time-dependent behavior of non-Newtonian fluids is represented by hardening. An example would be hardening (aging) of cement as it is being pumped into the subsurface during a grouting or well cementing job. In particular, if Bingham model is assumed for cement, both the plastic viscosity and the yield stress increase over time (Hässler et al., 1992). As an example, plastic viscosity vs time t was approximated with an exponential function in (Fidelibus and Lenti, 2012): $\mu_{pl} = \mu_{pl0}exp(\alpha t)$ where μ_{pl0} is the initial plastic viscosity; α is a time constant. A similar, exponential approximation was used also for the yield stress vs time in (Zou et al., 2018): $\tau_Y = \tau_{Y0}exp(\beta t)$ where τ_{Y0} is the initial yield stress; β is a time constant. Exponential approximations of time-dependent rheological properties may result in their excessively large growth over time. Therefore, alternatively, linear time-dependency may be assumed. Exponential approximations work well for a limited time, which is usually the case of interest in rock
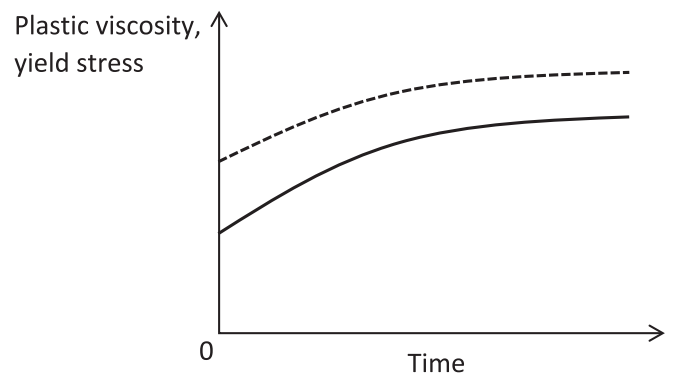

Fig. 8. Plastic viscosity (dashed line) and yield stress (solid line) vs shear time for a cement grout. Based on the experiments (Eriksson et al., 2000).

grouting applications (Zou et al., 2018). Rheological properties vs time curves measured in the experiments (Eriksson et al., 2000) follow a trend schematically shown in Fig. 8. This trend is neither linear nor is it given by the above exponential equations. It should rather be described by $y = y_\infty - (y_\infty - y_0)exp(-\gamma t)$ where $y = \mu_{pl}$ or $y = \tau_Y$, γ is a time constant (possibly different for μ_{pl} and τ_Y). Numerical modelling has shown a significant effect of hardening on the results of grouting jobs. In particular, the propagation distance of grout is affected (Hässler et al., 1992).

Time-dependent behavior is also characteristic of gel flow in fractures. When water originally present in gel leaks through the fracture wall, a concentrated immobile gel is left in the fracture (Seright, 2001).

Properly accounting for time-dependent behavior in fracture flow requires that the history of the fluid elements is traced. This can be achieved by using Lagrangian description of flow problems, whereby the equations of fluid mechanics are solved in a moving (Lagrangian) coordinate framework. Accounting for time-dependent effects in a fixed (Eulerian) coordinate framework is more challenging, and the accuracy is typically lower. A simplified Eulerian approach was employed in (Fidelibus and Lenti, 2012): instead of fluid elements, time-dependent properties were attributed to fixed grid points.

An important, for practical applications, class of non-Newtonian fluids is represented by suspensions of relatively large particles in a (Newtonian or non-Newtonian) carrier fluid. An examples would be a proppant-laden slurry pumped during hydraulic fracturing in order to maintain the fracture open after the injection is finished. As pointed out in (Tomac and Tartakovsky, 2018), flow of such fluids in long rough narrow fractures is not completely understood yet. Depending on the particle collision rate, flow can be dilute or collision-dominated. In a dilute regime, particles collide seldom, and their motion is dominated by the fluid drag force. In a collision-dominated regime, particle collisions affect their motion significantly. Another factor in particle suspensions is the lubrication force. It is a viscous dissipation force that prevents particles from approaching each other (or the fracture walls) and from moving away from each other (Lavrov and Laux, 2007). Lubrication force leads to particle agglomeration and may eventually lead to particles clogging the fracture aperture (Tomac and Gutierrez, 2015). Agglomeration is promoted by higher particle concentration and carrier fluid viscosity. All this complicates flow of particle suspensions in fractures even further.

The fracture flow models summarized in this Subsection have been derived for Stokes flow. An attempt to account for inertial effects in fracture flow of shear-thinning fluids (Carreau and Herschel-Bulkley) can be found in (Rodríguez de Castro and Radilla, 2017). Examples of advanced, fully 3D numerical simulations of inertial flows of shear-thinning fluids (Cross rheology) in a fracture digitized from a micro-CT image can be found in (Zhang et al., 2019).

2.2. Single-phase flow in a rough-walled fracture

So far, we have been concerned with flow between smooth, parallel plates. Roughness of real fracture surfaces introduces tortuosity in the fluid flow and, thus, additional complexity. Fluid flow in a fracture of variable local aperture is a three-dimensional process. A fully 3D modelling of such flows is time-consuming and only a few fully-3D computational fluid dynamics (CFD) studies of fracture flow of Newtonian (Brush and Thomson, 2003) and non-Newtonian (Zhang et al., 2019) fluids can be found. Therefore, two-dimensional models using the lubrication theory approximation (see below) are usually employed whereby the flow is averaged across the local aperture by means of the laws presented in Subsection 2.1. This reduces the compute time by two orders of magnitude, according to (Morris et al., 2015). The discrepancy in the hydraulic aperture obtained by lubrication theory approximation and by more accurate 3D CFD analysis is on the order of a few percent only (Lenci et al., 2022a).

To characterize the overall hydraulic conductance of rough-walled fractures, the concept of hydraulic aperture is used (Brown, 1987). For non-Newtonian fluids, hydraulic aperture can be defined as the aperture of a smooth-walled fracture that, under the same pressure gradient and with the same non-Newtonian fluid, produces the same flow rate as the rough-walled fracture does.

Fluid flow in rough-walled factures often occurs through few preferential flow paths of least flow resistance, a phenomenon known as channeling. Because of the fracture roughness and flow tortuosity, the hydraulic aperture is, in general, not equal to the mean aperture, i.e. the arithmetic average of the local fracture apertures (Wang et al., 2018).

A vast amount of literature is available on hydraulic conductivity of rough-walled fractures when the fluid is Newtonian. Analytical expressions for hydraulic aperture can be obtained only in some specific cases, e.g. when the aperture map has some sort of periodicity. In general, numerical modelling and experiments are invoked to investigate flow properties and hydraulic conductivity of rough-walled rock fractures. Numerical modelling boils down to solving the continuity equation

$$\nabla \cdot (w\mathbf{v}) = 0 \tag{29}$$

by means of finite-difference, finite-element or finite-volume methods. The so-called lubrication theory approximation is used for $\mathbf{v}$ by assuming that the cubic law holds *locally*. The lubrication theory has several underlying assumptions. In particular, it is assumed that the Reynolds number, Re, is small (Re $\ll$ 1), so that the flow is Stokes flow, and there are no recirculation zones between asperities. It is also assumed that the fracture faces are sufficiently smooth ($\nabla w \ll 1$). The latter implies that the ratio between the aperture variation and the shortest wavelength of the aperture profile is below a certain threshold value (Lenci and Chiapponi, 2020; Zimmerman et al., 1991). According to (Boronin et al., 2015), the lubrication approximation is valid as long as the product εRe is small (smaller than 1). Here, $\varepsilon = w/L$ where L is the in-plane length scale of the fracture. Under these conditions, Eq. (12) can be used for $\mathbf{v}$ for a Newtonian fluid.

Similarly to Newtonian fluids, in the case of non-Newtonian fluids, hydraulic aperture can be computed in closed form only for some simplest aperture maps. For instance, (Di Federico, 1997) analyzed flow of a power-law fluid in a fracture with sinusoidal variation of aperture along one direction. For such fractures, it was possible to obtain semi-analytical expressions for hydraulic aperture in two cases: when the flow is parallel or perpendicular to the aperture variation direction. Along the same lines, in (Lenci and Di Federico, 2020), semi-analytical expressions were obtained for a bi-viscous fluid in a fracture that has random variation of aperture in only one direction. In the general case of pressure gradient applied in an arbitrary direction, semi-analytical expressions cannot be obtained even for such oversimplified aperture maps. Also for more realistic, e.g. self-affine, aperture maps, the analytical approach does not work, and numerical modelling must be

used (Lavrov, 2013a). Here, again, Eq. (29) is solved by any available numerical method. The local velocity, $\mathbf{v}$, has in this case more complicated form than for Newtonian fluids, resulting in a nonlinear partial differential equation for the fluid pressure.

Experimental verification of the numerical solutions for non-Newtonian fluid flow in a single fracture is of great interest because there are a number of assumptions underlying the numerical models. In particular, the applicability range for the lubrication approximation, still debated even for Newtonian fluids, has not been analyzed for non-Newtonian fluids at all. Experiments could validate or invalidate the use of this approximation and numerical models based thereon. Such experiments require bespoke equipment and are rare. Typical equipment for such experiments is a Hele-Shaw cell. A Hele-Shaw cell consists of two transparent plates parallel to each other. The distance between the plates can be changed and roughness or undulation can be introduced to the plates' inner sides. The distance between the plates (the aperture) is much smaller than the in-plane dimensions of the plates. An experiment of this type was reported in (Lenci and Chiapponi, 2020). A Hele-Shaw cell with one of the plates having random undulations in the direction of flow represented effectively a one-dimensional aperture profile. The flow rate through the cell was calculated numerically for Newtonian and power-law fluids whereby the rheological parameters for the latter were obtained with a rheometer. Flow experiments were performed with both Newtonian and power-law fluids. The numerical model with lubrication approximation agreed well with the experiment for Newtonian fluid but, in all but one cases, underestimated the flow rate by a factor up to 2 for non-Newtonian fluids. The discrepancy between experiment and theory in the latter case was attributed to two possible reasons: (i) the limited range of shear rates allowed by the rheometer and (ii) slip at the walls (no-slip boundary conditions are used at the fracture faces in numerical models, just as they were assumed in the theoretical models summarized in Section 2.1). In addition, the power-law model might not be valid for non-Newtonian fluids used in the experiments: the only experiment where the flow rate of non-Newtonian fluid was predicted correctly was the one where the fluid was likely to have a nonzero yield stress (Lenci and Chiapponi, 2020). Experiments with fracture flow of non-Newtonian fluids require that the distance between the plates (i.e. the fracture aperture) be controlled precisely since the aperture has a significant effect on the flow rate, due to the cubic law. One of the challenges here is that, if the plates are not sufficiently stiff, the aperture varies with the fluid pressure which introduces a parasitic component into the aperture profile along the flow direction (Majidi et al., 2010a). Experiments with radial flow of non-Newtonian fluids into a Hele-Shaw cell (representing radial flow of drilling mud or cement grout into a fracture) have been reported in (Funehag and Thörn, 2018; Majidi et al., 2010a).

2.2.1. Hydraulic aperture is a function of rheological properties for non-Newtonian fluids

Even for the simplest non-Newtonian rheology, a power-law fluid, the hydraulic aperture depends not only on the aperture distribution of the fracture but also on the fluid properties (Lenci et al., 2022b). This is remarkably different from Newtonian fluids where the hydraulic aperture is independent of the fluid viscosity and is, thus, a intrinsic property of the fracture.

To illustrate the dependency of hydraulic aperture on fluid rheology, I will use a model of power-law fluid flowing in the *x*-direction, along a sinusoidal one-dimensional aperture profile given by:

$$w_h = w_m \left(1 + \delta sin\frac{2\pi x}{\lambda}\right) \tag{30}$$

where w_m is the mean aperture; δ is a dimensionless parameter characterizing the magnitude of the aperture variation. The hydraulic aperture can in this case be evaluated semi-analytically as follows (Di Federico, 1997):
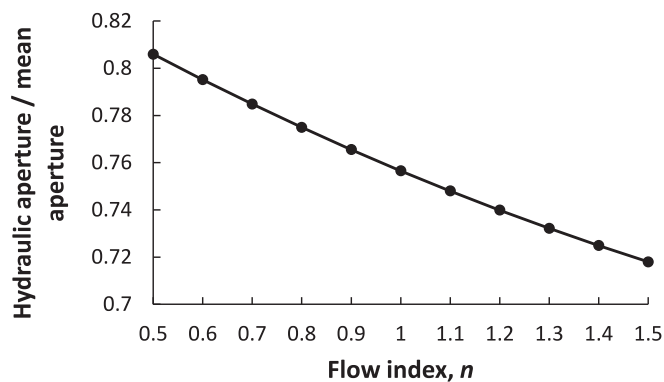
Fig. 9. Hydraulic aperture normalized by the mean aperture, w_h/w_m, vs. the flow index of a power-law fluid. Flow along a one-dimensional sinusoidal profile given by Eq. (30) with $\delta = 0.5$.

$$w_h = w_m \left[\frac{1}{\lambda} \int_0^\lambda \frac{dx}{\left(1 + \delta sin\frac{2\pi x}{\lambda}\right)^{2n+1}} \right]^{-1/(2n+1)} \tag{31}$$

where n is the flow index of the power-law fluid. According to Eq. (31), hydraulic aperture should depend on the flow index, n. This is illustrated in Fig. 9 for $\delta = 0.5$.

Also for other types of non-Newtonian rheology the hydraulic aperture can be shown to depend on the rheological parameters of the fluid and not just be a function of the aperture map.

Numerical modelling suggests that, as the fluid becomes more shear-thinning, the fracture becomes more permeable compared to the case when the fluid is Newtonian (Lenci et al., 2022b). This is also illustrated by the above simple one-dimensional model (Fig. 9) when n is smaller than 1.0. In a two-dimensional, rough-walled fracture, this increase is even more pronounced and is attributed to the fact that shear-thinning rheology enhances the flow channeling which, in turn, reduces viscous dissipation in the fluid (Lenci et al., 2022b). Enhancement of flow channeling is the subject of the next Subsection.

2.2.2. Shear-thinning enhances flow channeling

Channeling is commonly observed when Newtonian fluids flow in rough-walled fractures. The phenomenon is due to the fact that flow often occurs through a few preferential paths of lowest resistance. Preferential flow paths, flow anisotropy and channeling are especially pronounced in fractures that have experienced shear displacement (Koyama et al., 2006). Shear-thinning rheology enhances flow channeling (Lavrov, 2013b; Lenci et al., 2022a; Zhang et al., 2019) and the development of preferential pathways (Lenci et al., 2022b; Rodríguez de Castro and Radilla, 2017). The enhanced channeling has been observed in experiments with shear-thinning solutions flowing in rough-walled artificial fractures (Auradou et al., 2008).

The observed enhancement of channelization in shear-thinning fluids can be explained as follows (Zhang et al., 2019): In a rough-walled fracture, a fluid (Newtonian or non-Newtonian) flows through preferential flow paths, i.e. "channels". For any fluid, Newtonian or not, the fluid velocity is larger at locations with a larger aperture. Larger velocity induces larger shear rate. For a shear-thinning fluid, this results in a reduced apparent viscosity, which, in turn, will *additionally* increase the fluid velocity in these large-aperture channels (*additionally* as compared to a Newtonian fluid for which the apparent viscosity does not depend on the shear rate). Therefore, channelization is enhanced for shear-thinning fluids (Rossen and Kumar, 1992). It should be noted that, in inertial flows, this effect is counteracted by an increase in tortuosity at high Reynolds numbers, and a shear-thinning fluid might in fact show the same degree of channelization as a Newtonian fluid at the same high *Re* (Zhang et al., 2019).
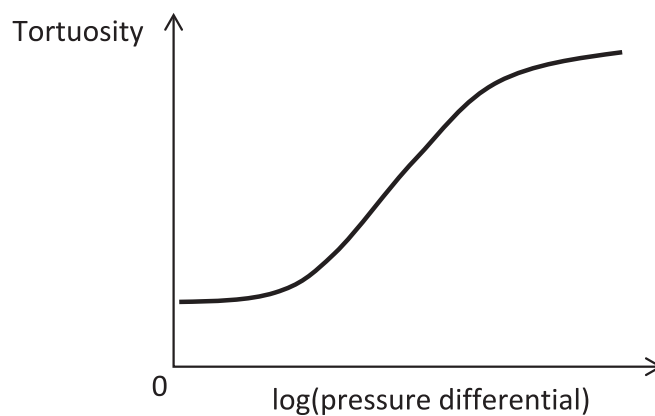
a
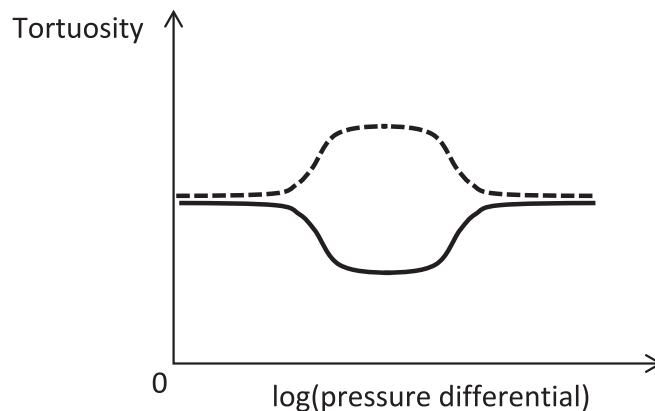
b

Fig. 10. Flow tortuosity as a function of pressure differential for Bingham fluid (a), shear-thinning truncated power-law fluid (b, solid line) and shear-thickening truncated power-law fluid (b, dashed line). Based on (Bao et al., 2017).

In numerical simulations, channeling can be quantified by computing the flow tortuosity. Tortuosity, T, is usually defined as the ratio of the mean fluid velocity magnitude to the mean value of the velocity component parallel to the general flow direction (Koponen et al., 1996; Lavrov, 2021b; Zhang et al., 2019). For a Newtonian or non-Newtonian fluid flowing between smooth parallel walls, $T = 1$. For flow in a rough-walled fracture, $T > 1$. If the flow were channeled through a few straight pathways, tortuosity would be equal to 1. Thus, channeling can be quantified by a decrease in tortuosity.

For a Newtonian fluid and non-inertial flow, tortuosity does not depend on the magnitude of the applied pressure differential and could be considered a fracture property (though it might depend on the *direction* in which the pressure differential is applied, i.e. on the general direction of flow). The situation is different for non-Newtonian fluids: tortuosity in this case depends on the magnitude of the applied pressure differential or, equivalently, on the magnitude of the Reynolds number (Zhang et al., 2019). For instance, for a Bingham fluid, as the applied pressure differential is increased, tortuosity increases, i.e. the flow becomes less channeled (Fig. 10a). This happens because, as the pressure differential increases, the effect of the yield stress is reduced, and the

fluid behaves more and more like a Newtonian fluid.

A direct impact of rheology on flow channeling was observed in numerical simulations of Bingham fluids having different yield stress values. It was obtained that increasing yield stress increases channeling (Hanssen, 2013). This is consistent with the behavior shown in Fig. 10a.

Another example of tortuosity being enhanced by shear-thinning rheology is obtained with a shear-thinning truncated power-law fluid (Fig. 10b, solid line). In this case, the tortuosity is higher at very low and very high pressure differentials, when the fluid behaves like a Newtonian fluid. In the middle range of pressure differential, when the fluid behaves like a power-law fluid, tortuosity is lower, i.e. the flow is more channelized.

The situation is opposite for a shear-thickening truncated power-law fluid (Fig. 10b, dashed line). In this case, tortuosity is highest at intermediate pressure differential values. Accordingly, flow becomes more channeled at very low and very high pressure differentials, where the fluid behaves like a Newtonian fluid (which is "thinner" than the shear-thickening fluid obtained at intermediate pressure differentials).

2.2.3. Yield stress creates immobile-fluid zones (trapped fluid)

Non-Newtonian rheology with yield stress may lead to a peculiar phenomenon in fracture flow, namely trapped (immobile) fluid. This happens where the local pressure gradient drops below $2\tau_Y/w$. In such zones, the unyielded core occupies the entire fracture aperture, and the flow locally stops. In a numerical simulation, this introduces a new boundary. One way to circumvent this problem in a numerical simulation is to introduce a negligible nonzero conductivity at the location where the flow condition, $|\nabla P|\rangle 2\tau_Y/w$, is not met (Morris et al., 2015). Another solution to the problem is to use regularized fluid rheology, as discussed above.

When a yield-stress fluid is injected from a borehole into a horizontal fracture while keeping the borehole pressure constant, the flow will eventually stop. This happens because, in a radial flow, the average fluid velocity decreases with the distance from the injection point (i.e. the borehole), due to mass conservation. As a result, the unyielded plug occupies a greater fraction of the aperture as the distance from the injection point increases. Eventually, the plug will occupy the entire fracture aperture at the front of the invading yield-stress fluid, and the flow will stop. This effect was analyzed theoretically and observed experimentally (Majidi et al., 2010a).

As mentioned above, a yield-stress fluid stops flowing in a fracture when the local pressure gradient becomes smaller than $2\tau_Y/w$ (Grindrod et al., 1999). This may happen even if the fluid does not contain any suspended solid particles. When the fluid contains solids, there is an additional mechanism that can stop the flow, namely build-up of a filter cake (a plug) upstream of a flow constriction. Experiments show that, when a yield-stress fluid flows through a constriction (a narrowing in the aperture), solid particles gradually build up both upstream and downstream the location of the constriction (Draganović and Stille, 2014). Solid particles are deposited in the fracture because they cannot freely pass the constriction. The carrier fluid can still be filtered through the filtercake but the rheological properties of the filtrate (the diluted suspension) will be different from the original suspension (Eriksson et al., 2000). One way to conceptualize the process of filtercake buildup in this setting is to introduce two threshold values for the fracture aperture: $w_{critical}$ and w_{min}. When $w > w_{critical}$, the suspension can pass without filtercake deposition. When $w_{min} < w < w_{critical}$, filtercake is deposited. When $w < w_{min}$, there is no flow (Eriksson et al., 2000; Mohajerani et al., 2015).

It is not uncommon that a narrow channel may remain through the filtercake, and the fluid containing solid particles could still continue flowing through the channel, a process known as "pinholing" (Cerasi et al., 2001). Channels may get blocked and new channels may appear. In any event, conductivity of the fracture is reduced compared to the case without filter cake deposition.

Both processes contributing to immobile fluid, i.e. nonzero yield

stress and particle deposition, are controlled by the fracture aperture. One commonly used rule of thumb says that particles can bridge a fracture when the fracture aperture is smaller than 2.5 times particle diameters. A broader particle size distribution facilitates bridging (Lavrov, 2016, 2017b; Lohne et al., 2010).

Completely plugging a fracture by immobile (trapped) yield-stress fluid becomes more difficult when the aperture distribution becomes wider, i.e. when the standard deviation of the aperture distribution increases (Rossen and Kumar, 1992). This is due to the presence of wider channels in a fracture of a wider aperture distribution. As a result, the penetration distance of a yield-stress fluid pumped into a rough-waled fracture is greater when the standard deviation of the fracture aperture is larger (Gustafson and Stille, 1996).

2.3. Two-phase flow and displacement

In applications, a situation is common where a non-Newtonian fluid displaces a Newtonian formation fluid or another non-Newtonian fluid. For instance, in tunnel grouting, cement (a yield-stress fluid) displaces water. Similar process takes place in drilling, with a drilling fluid (a yield-stress fluid) displacing a Newtonian formation fluid. In hydraulic fracturing, several non-Newtonian fluids may be pumped one after another into the fracture.

Even when both, displacing and displaced, fluids have Newtonian rheology, the process is quite complex. Theoretical analysis of such flows in a Hele-Shaw cell with smooth parallel walls was first carried out by Saffman and Taylor in 1958 (Saffman and Taylor, 1958). Conditions for stable and unstable displacements were derived using linear stability analysis. In particular, it was shown that, in a horizontal cell, the displacement is stable when the dynamic viscosity of the displacing fluid is larger than that of the fluid being displaced. In the opposite case, instability of the displacement front in form of fingering occurs.

Similar to the seminal work of Saffman and Taylor, most analytical studies of two-phase flows in Hele-Shaw cells, including those that involve non-Newtonian fluids, are based on a number of simplifying assumptions. Namely, the aperture is much smaller than the other two dimensions in the system (along and normal to flow); the fluid velocity component normal to the cell walls is negligible; the rate of variation of the velocity in the direction normal to walls is much larger than in the other two directions. In addition, the fluids are typically assumed incompressible, and inertia is assumed negligible. An example of work done using the above assumptions for Hele-Shaw cell flow involving two Herschel-Bulkley fluids can be found in (Coussot, 1999). It was, in particular, obtained that, when gravity effects are negligible, unstable displacement occurs when the wall shear stress is smaller in the displacing fluid, i.e. when the displacing fluid is less viscous. Further discussion of stable vs. unstable displacement involving non-Newtonian fluids follows below in this Subsection.

Some theoretical insights into non-Newtonian two-phase flow in fractures can be gained from similar studies performed for porous media. For instance, in (Pascal, 1984), displacement of a Bingham fluid by another Bingham fluid in porous media was considered. The flow equation for a Bingham fluid in porous media was assumed to have the same form as the linearized equation for the Bingham fluid [see text after Eq. (18)]. Stability criteria were derived. It should be noted, however, that direct applicability of porous media theory to fracture flow might be questionable since, in the case of non-Newtonian fluids, the flow rate vs. pressure gradient law has a slightly different form for the two.

Experiments on two-phase flows in fractures involving non-Newtonian fluids are rare. An example is a recent work of (Taheri et al., 2021) where 16 tests were performed in a large, 1 m × 0.6 m, Hele-Shaw cell with smooth parallel plates. Various combinations of displaced and displacing fluids were used, with either one or both fluids being yield-stress fluids (in addition to Newtonian-Newtonian displacement tests). Another example of experimental work is the
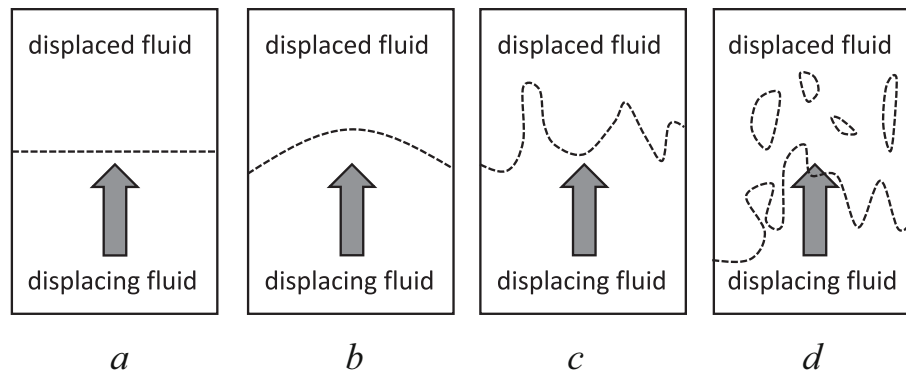
Fig. 11. Three types of fluid displacement in a Hele-Shaw cell in two-phase flow of Newtonian/non-Newtonian fluids: stable, piston displacement (a), viscous fingering (b, c) and bubble flow displacement (d). Dashed line shows the interface between the two fluids. Arrow shows the predominant flow direction.

thorough study by Boronin et al. (Boronin et al., 2015).

Numerical studies of two-phase flows involving non-Newtonian fluids in rough-walled fractures are rare as well. An example of such modelling study is (Morris et al., 2015). Here, the authors used a Lagrangian method to track interfaces as several fluid of various rheology (Newtonian and non-Newtonian) were injected into the fracture.

Often, when modelling displacement of the formation fluid (e.g. water) by a non-Newtonian yield-stress fluid (e.g. cement grout), modelers assume that the viscosity of the former is negligible. This reduces the problem to a single-phase flow with a moving front, as e.g. in (Liu et al., 2021). It was shown in (Zou et al., 2018) that this approach is viable only when the viscosity contrast between the two fluids is large, i. e. the grout viscosity is relatively high. Otherwise, replacing two-phase flow with a single phase may introduce errors in excess of 20% into the grout penetration distance. In the mudloss model of (Dokhani et al., 2020), replacing two-phase flow by single-phase was found to affect especially the initial stages of a mudloss event.

It should, finally, be noted that analytical, numerical, and experimental studies of non-Newtonian two-phase flow in fractures have typically been conducted under restrictive assumptions of lubrication approximation and non-inertial flow. It has been speculated that he same flow regimes should be relevant for fracture flow as for pipe flows, including stratified flow, annular flow, intermittent flow etc. (Ma et al., 2017). Experimental and theoretical verification of this hypothesis is an outstanding research task.

2.3.1. Displacement regimes in low-Re two-phase flows with non-Newtonian fluids

Experiments of (Taheri et al., 2021) revealed three displacement regimes in two-phase fracture flows involving non-Newtonian fluids:

- stable, piston-like displacement;
- viscous fingering;
- bubble-flow displacement.

They are schematically illustrated in Fig. 11.

Stable, piston-like displacement in a vertical Hele-Shaw cell takes place when the displacing fluid injected into the bottom of the cell is both heavier and has a higher apparent viscosity than the fluid in place. In this case, the interface remains flat and stable during displacement, and the injected fluid replaces the original fluid uniformly across the entire cell (Fig. 11a). This regime ensures the most effective displacement, with very few pockets of trapped original fluid left in the cell (the pockets are due to wettability conditions on the walls of the cell, see further in this Subsection). This regime is often assumed in numerical models when one is primarily interested in displacement of a Newtonian fluid by a yield-stress fluid. For instance, piston-like displacement was

assumed in a numerical models of mud losses into a horizontal fracture initially filled with a Newtonian formation fluid (Lavrov, 2022; Majidi et al., 2010b). This assumption enabled treatment of the problem as a one-dimensional, radial flow problem. Another example is a two-dimensional DFN model of grouting where a Bingham cement displaces the formation fluid (Fidelibus and Lenti, 2012). As long as more complicated local scenarios are not allowed, e.g. displacement of cement by water, the piston-displacement model can be a good approximation.

Viscous fingering (Saffman-Taylor instability) was observed in a horizontal Hele-Shaw cell when a Newtonian fluid was displacing a yield-stress fluid (Boronin et al., 2015). The undisplaced yield-stress fluid may remain immobile during the displacement and thus be trapped behind the displacement front. Fingering in a vertical, upward displacement in a vertical Hele-Shaw cell is observed e.g. when a slightly heavier Newtonian fluid displaces a yield-stress fluid with a sufficiently higher apparent viscosity. Depending on the flow rate, viscous fingering in this case can assume a shape of a single wide finger (at lower flow rates, Fig. 11b) or several narrow fingers (at higher flow rates, Fig. 11c) (Taheri et al., 2021). Fingering is also observed when a slightly heavier yield-stress fluid displaces a slightly lighter yield-stress fluid of a sufficiently higher apparent viscosity. Fingers are less pronounced in this case than in the case of Newtonian displacing fluid (Taheri et al., 2021). In (Boronin et al., 2015), both experiments and numerical simulations demonstrated that, when a Newtonian fluid is injected into a yield-stress fluid filling the cell, the displacement may look like a single narrow finger (a channel) penetrating through the unyielded yield-stress fluid. A shielding effect is observed: longer fingers are favored; shorter fingers are stopped. This segregation of fingers is more pronounced at higher Bingham numbers, Bn. The Bingham number in fracture flow is defined as follows: $Bn = \tau_Y w / v \mu_a$ where v is a characteristic velocity; μ_a is apparent viscosity that corresponds to v.

Viscous fingering may occur even when the flow originally was single-phase. For instance, dehydration of a gel as it flows through a fracture results in formation of a concentrated, immobile gel. Non-dehydrated gel being injected into the fracture may then develop wormholes through the concentrated gel (Seright, 2001).

In addition to fingering in the plane of the fracture, illustrated in Fig. 11b, c, fingering in these scenarios is observed also across the fracture aperture. For instance, when a yield-stress fluid displaces another yield-stress fluid in a horizontal fracture, and the apparent viscosity of the displacing fluid is lower, a finger develops across the aperture (Fig. 12). As a result, layers of undisplaced yield-stress fluid are left near the walls. The fraction of the fluid left on the walls depends on the yield stress of the displaced and displacing fluids, and decreases with either (Freitas et al., 2013). Similarly, when the displacing fluid is Newtonian and the fluid in place is a shear-thinning non-Newtonian fluid with a higher apparent viscosity, or a yield-stress fluid, fingering similar to the one shown in Fig. 12 is predicted (Morris et al., 2015). In
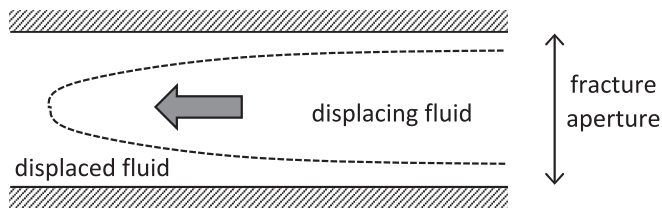
Fig. 12. Fingering in the plane spanned by the fracture aperture and the flow direction. Both displaced and displacing fluids are yield-stress fluids. Apparent viscosity of the displacing fluid is lower than that of the displaced fluid. Dashed line shows the interface between the two fluids. Arrow shows the predominant flow direction.

the case of a yield-stress fluid in place, a static layer (a film) of this fluid remains on the walls after the injected Newtonian fluid has traversed the fracture (Boronin et al., 2015). Fingering shown in Fig. 12 creates effectively a "mixing zone" where the two fluids coexist in the same vertical cross-section (Mehr et al., 2020).

Bubble-flow displacement can be observed in a vertical, upward Hele-Shaw flow when a yield-stress fluid displaces a slightly heavier Newtonian fluid (Fig. 11d). The displacement in this case happens in form of droplets of the displacing yield-stress fluid rising through the heavier Newtonian fluid in place (Taheri et al., 2021).

Further experiments are needed in order to investigate whether the above three flow regimes – piston-like, fingering, and bubble flow – are the only regimes that can be observed in Hele-Shaw cell experiments involving non-Newtonian fluids, even at low Reynolds numbers. Furthermore, robust quantitative criteria for prediction of the flow regimes need to be established, by using either experiments or numerical (or analytical) models. It should be noted that for flows involving only Newtonian fluids elaborate instability models are already available that enable quantitative prediction of the interface evolution (Foroushan et al., 2018).

Viscous fingering in experiments with non-Newtonian fluids described above is, in some ways, similar to viscous fingering observed when a Newtonian fluid displaces another, more viscous, Newtonian fluid (cf. the original Saffman-Taylor work). There are, however, some differences. In particular, when the fluid being displaced is a shear-thinning non-Newtonian fluid, the apparent viscosity at the finger tip (where the shear rate is largest) is lower than in the body of the finger. Numerical modelling shows that this suppresses the splitting at the finger tips and produces narrow fingers (Kondic et al., 1998). These narrow fingers are consistent with those found in the experiments where shear-thinning polymer solutions were displaced by air (Lindner et al.,
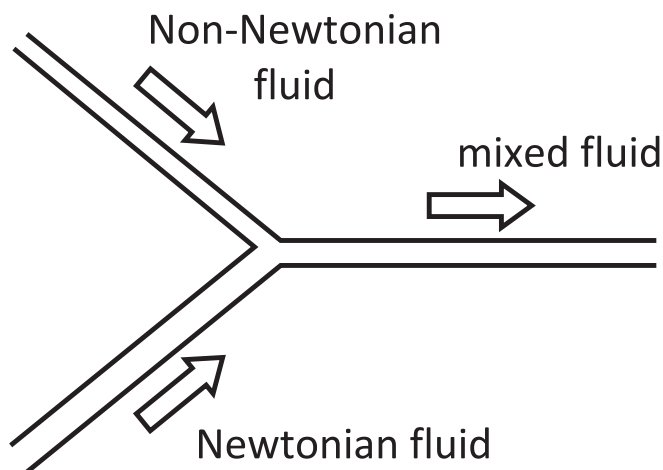
2002). Numerical modelling of (Kondic et al., 1998) also showed that side branching and oscillations of the interface are enhanced when the fluid being displaced is shear-thinning.

Experiments in Hele-Shaw cells with a Newtonian fluid displacing a shear-thinning fluid corroborated the above modelling results and confirmed that non-Newtonian rheology introduces extra complexity in the flow instabilities (Hallot et al., 1996). To characterize the flow regime, a non-dimensional number given by $B^{-1} = 12L^2\mu_a\nu/Tw^2$ can be used. Here, L is the width of the cell; T is the surface tension; μ_a is the apparent viscosity of the non-Newtonian fluid in place. At relatively small B^{-1} ($B^{-1} < 10^4$), usual Saffman-Taylor instabilities were observed. At higher values of B^{-1} (B^{-1} about 10^6), fingers gave rise to dendritic structures, with a fractal dimension of 1.7. It was noticed that dendritic structures only developed in Hele-Shaw cells with sufficiently small gaps. Increasing B^{-1} above 10^6 resulted in cracks with sharp tips propagating in the non-Newtonian fluid. This displacement regime is unique for non-Newtonian fluids. Thus, flow regimes vary from viscous flow through viscous fingering through dendritic structures to crack propagation when a shear-thinning fluid is displaced by a Newtonian one (Hallot et al., 1996).

Recent experiments of (Mehr et al., 2020) revealed additional complexity in miscible displacement involving a shear-thinning fluid. In those experiments, a shear-thinning solution (xanthan gum) was displacing Newtonain saltwater in radial flow in a Hele-Shaw cell. Such displacement is expected to be stable, i.e. piston-like. Experiments demonstrated, however, that an irregular, wavy interface developed between the two fluids. This effect was enhanced in cells of smaller aperture and in experiments with a higher flow rate.

Numerical models of two-phase flow and displacement in fractures are rare. One example is (Boronin et al., 2015) where both the theoretical model and the numerical algorithm used to solve it are described in great detail.

2.3.2. Trapped fluid

Even when the displacement is piston-like, pockets of the original fluid may be left in place behind the displacement front. Such pockets of bypassed trapped fluid were observed in Hele-Shaw experiments where both fluids were Herschel-Bulkley fluids with the same flow index and consistency index but different yield stress and density: the displaced fluid was slightly lighter and had a lower yield stress, 0.16 Pa vs. 0.39 Pa of the displacing fluid (Taheri et al., 2021). Despite the displacing fluid being heavier and more viscous, pockets of the displaced fluid were left after the displacement front had passed through the cell. The entrapment was reduced by wetting the plate surfaces with the displacing fluid before the experiment started.

Fluid bypass and entrapment are enhanced when the displacement regime is unstable, i.e. when fingering occurs (Fig. 11b, c). Particularly low displacement efficiency is observed in bubble-flow displacement (Fig. 11d).

3. Flow of non-Newtonian fluids in fracture networks

In a two-dimensional DFN, each fracture is represented by a line segment, typically a straight line. In a three-dimensional DFN, each fracture is usually represented as a polygon or an ellipse. A comprehensive review of using DFN for fracture modelling is outside the scope of this paper. The interested reader is referred to e.g. (Hyman et al., 2016; Lei et al., 2017).

Flow of Newtonian fluids in fracture networks has been studied extensively for the past 50 years. These studies, mostly by numerical modelling, revealed, in particular, that, depending on the properties of the network, flow can be more or less uniform, be channeled through a few fracture paths, or be channeled through a single fracture path (de Dreuzy et al., 2002).

Fracture network flows involving non-Newtonian fluids present similar challenges as fracture network flows involving only Newtonian

Fig. 13. Non-Newtonian fluid and Newtonian fluid flowing into a Y-junction simultaneously.

fluids (Berre et al., 2019). Some additional issues are due to non-Newtonian rheology.

3.1. Flow at fracture intersections

Modelling flow at fracture intersections is complicated even in the case of single-phase Newtonian fluid flow in a 2D network (Boon et al., 2018). In the case of two-phase flow (in either 2D or 3D network) and non-Newtonian rheology, problems are exacerbated. Firstly, in the case of even 2D network, it is not clear how to model the flow when two fluids with different rheologies meet at an intersection (Fig. 13). In the case when both incoming fluids are Newtonian, some simple mixing rules could be assumed. For instance, in (Ma et al., 2018), viscosity and density of the mixed fluid were computed as weighted averages of the properties of the incoming fluids:

$$\rho_m = \lambda_1 \rho_1 + \lambda_2 \rho_2 \tag{32}$$

$$\mu_m = \lambda_1 \mu_1 + \lambda_2 \mu_2 \tag{33}$$

where subscripts "1" and "2" refer to the fluids flowing towards the Y-junction; subscript "m" refers to the mixed fluid leaving the Y-junction; ρ is density; μ is viscosity; λ is the ratio of the flux of fluid "1" or "2" to the total flux.

When one of the fluids, "1" or "2", is non-Newtonian, Eq. (33) can no longer be used, and the mixing law for rheological properties of the "mixed fluid" should be developed. Literature review reveals no attempts to derive such mixing laws. An averaging approach similar to the above approach of (Ma et al., 2018) was used when modelling two-phase non-Newtonian/Newtonian flows in (Morris et al., 2015): local fracture conductivity was assumed to be a weighted average (by the volume fraction) of the conductivities that would be obtained with each of the phases occupying the entire fracture aperture.

In a situation shown in Fig. 13, mixing would be taking place continuously at the intersection. It means that a new interface should be introduced at each timestep. This would effectively increase the number of interfaces (and thus the number of degrees of freedom) ad infinitum if interfaces were not leaving the fracture downstream. In order to simplify the mixing algorithm, different roads have been taken in numerical models. For instance, in (Hässler et al., 1992), only 10 dilution levels were allowed when non-Newtonian grout was mixed with water at an intersection in a 2D DFN. To simplify the treatment of mixing even further, some DFN models neglect the effect of mixing on the density. For instance, in a displacement of water by non-Newtonian cement grout, the mixture density was assumed to be equal to the density of the grout (Fidelibus and Lenti, 2012).

Two-phase flow at fracture intersections is considerably more complicated in three-dimensional fracture networks. Firstly, flow *along* the intersection becomes possible. Secondly, due to viscous fingering and flow channeling in each fracture, the displacing fluid may reach different parts of an intersection at different times, i.e. breakthrough at different locations happens at different times. Thirdly, mixing laws involving non-Newtonian fluids are not available. The first issue, flow along an intersection, can be treated as a pipe flow, just as it is done for Newtonian fluids (Berre et al., 2019). The second issue, due to possible viscous fingering and channeling inside each fracture, may introduce a considerable complexity in the flow pattern at an intersection, such as an early breakthrough illustrated in Fig. 14. In addition to viscous fingering in the plane of the fracture, shown in Fig. 14, early breakthrough may be due to viscous fingering in the plane normal to the fracture plane. Viscous fingering, either in the fracture plane or in the plane normal to it, happens e.g. when water is injected into a fracture containing a more viscous shear-thinning fluid (Fig. 12). Numerical simulations show that water in this case penetrates along the middle plane of the fracture aperture, between the layers of the non-Newtonian fluid (Morris et al., 2015). Another factor contributing to early breakthrough shown in
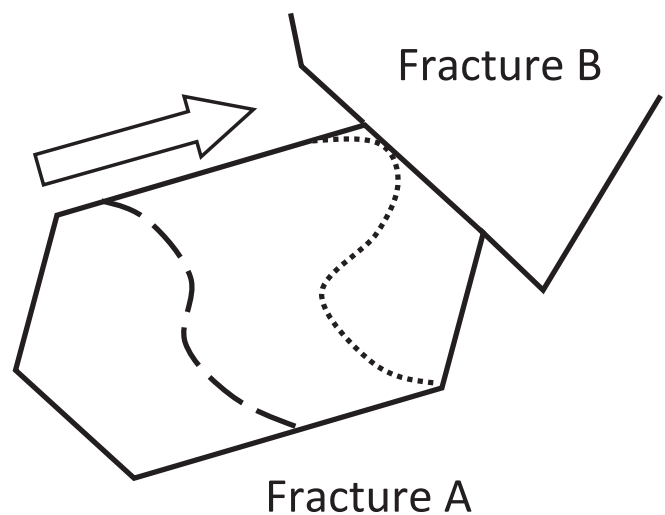
Fig. 14. Front of displacing fluid reaching an intersection in a 3D DFN at different times at different locations. Dashed and dotted lines show position of the displacement front at an earlier and later time, respectively.

Fig. 14 is flow channeling caused by fracture roughness (Subsection 2.2). A shear-thinning fluid travelling through the channels is likely to arrive at the intersection earlier than the rest of the fluid, which will result in a pattern similar to the one shown in Fig. 14. In addition to viscous fingering and roughness-related channeling, another factor that enhances flow complexity in a fracture network is irregular geometry of the intersections caused by variation in the local aperture of the intersecting fractures (Zou et al., 2017).

Experimental study of flow patterns developing at fracture intersections in three-dimensional networks is complicated. A notable example of such experiments is the recent work by (Ma and Tomac, 2021) where flow of a proppant-laden slurry through a fracture junction was investigated. It seems to be a general consensus in the research community that numerical modelling is a viable research avenue here. However, even numerical studies with Newtonian fluids are rare and usually involve considerable simplifications. For instance, finite-element simulations of steady incompressible single-phase laminar flow of a Newtonian fluid in a 3D fracture network composed of five intersecting fractures was performed in (Aghajannezhad et al., 2021). It was found that increasing the length of the intersections increases the flow rate through the network.

Knowledge gaps related to flow at intersections need to be addressed in order to perform meaningful simulations of non-Newtonian (and Newtonian) fluid flows in 3D DFNs. Three-dimensional DFN models are essential because, in 3D, fluids can flow along intersections, and there are more low-resistance pathways through the network than in 2D (Zou et al., 2019). As a consequence, a 2D model is likely to underestimate the hydraulic conductivity of a fractured rock mass.

3.2. Tracking the displacement front in two-phase flow

In a two-phase flow, the interface between the invading fluid and the fluid in place must be tracked throughout the simulation. This is especially difficult in 3D because of fingering and channeling, as illustrated
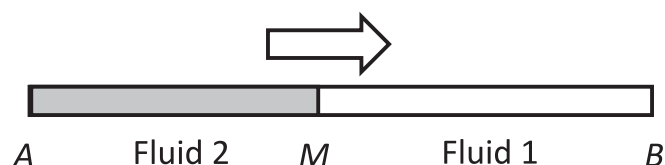
Fig. 15. Flow in a fracture embedded in a two-dimensional DFN.

in Fig. 14. But even in 2D fracture networks, interface tracking is a challenge. The interface is usually assumed to be sharp in 2D DFN models (Hässler et al., 1992). But even under this assumption, interface tracking is still challenging. Numerical manifold method was used in (Ma et al., 2018) to handle interface movement in a two-phase flow involving two Newtonian fluids in a 2D DFN. Each interface introduces an additional degree of freedom. New interfaces constantly appear at intersections as fluids get mixed into mixtures having different properties. As a result, the number of degrees of freedom in the simulation may increase throughout the simulation. Properly handling this scenario may require prohibitively small timesteps if accuracy is to be maintained (Lavrov, 2021a). The issue of increasing number of degrees of freedom can be addressed by introducing extra simplifications in the model. For instance, in (Zou et al., 2019), at most one interface was allowed in each fracture.

3.3. Computational extra cost due to nonlinearity

Nonlinear behavior of non-Newtonian fluids, with the flow rate being a nonlinear function of the pressure gradient, increases the computational cost of a network flow simulation. Consider, for instance, a fracture embedded in a two-dimensional DFN model (Fig. 15). Consider first the case where two *Newtonian* fluids are present in the fracture, e.g. fluid 1 from node *A* (end of the fracture) to point *M*, and fluid 2 from point *M* to node *B* (the other end of the fracture). In this case, an analytical solution exists for the pressure at point *M*, given the pressure values at the fracture ends *A* and *B*. Moreover, the breakthrough time (the time needed for the interface to move from *A* to *B*), can be calculated analytically in closed form (Lavrov, 2021a).

All this changes when fluid 2 is non-Newtonian. In this case, the displacement should still be piston-like. However, there is no closed-form solution for the pressure at the interface in this case. An iterative procedure must be used to obtain pressure at point *M* (Fidelibus and Lenti, 2012). Iterations required to obtain the interface pressures slow down the DFN simulation. Moreover, the breakthrough time cannot be calculated in closed form (Lavrov, 2021a) which makes it difficult to adjust the timestep in a DFN simulation.

3.4. Fracture-matrix fluid exchange

The description of fracture-matrix fluid exchange is not trivial even for Newtonian fluids, and several different models are in use (Unsal et al., 2010). For instance, in (Berre et al., 2019; Martin et al., 2005), the use of the following equation for flow through the fracture wall was advocated:

$$v_n = \frac{k_n}{\mu} \frac{P - P_m}{w/2} \tag{34}$$

where v_n is the fluid leak-off velocity (superficial fluid velocity) normal to the fracture wall; P_m is the fluid pressure in the rock matrix near the fracture wall; k_n is the "permeability in the normal direction" (Martin et al., 2005). The latter represents "the equivalent resistivity across the fracture".

Equations similar to Eq. (34) could, in principle, be constructed for non-Newtonian fluids as well. In practice, however, simple empirical models of the leak-off rate are often employed for non-Newtonian fluids. An example is Carter's law widely used in hydraulic fracturing and mud loss models (Dokhani et al., 2020; Valkó and Economides, 1995). According to Carter's law, the leak-off rate has two components: a "spurt loss" that takes place instantaneously as the incoming fluid reaches a given location in the fracture, and a gradually decaying time-dependent component (Adachi et al., 2007; Valkó and Economides, 1995):

$$v_n = 2Q\delta(t - t_0) + \frac{2C_L}{\sqrt{t - t_0}} \tag{35}$$

where *Q* is the spurt loss through the fracture wall; δ is the delta-function; t_0 is the time when the fluid reaches a given location in the fracture, and the leak-off commences; C_L is an empirical leak-off coefficient. The factor of two is used in both terms on the right-hand side of Eq. (35) because the fracture has two permeable faces.

Validity of Eq. (35), and in particular the value of the exponent in the time-dependent term ($-1/2$), near the tip of a propagating hydraulic fracture was disputed in (Wrobel and Mishuris, 2015).

Leak-off is a complicated process that results in the formation of external and internal filtercake on the rock face (Caenn et al., 2011). The filtercake makes the fracture-rock interface less permeable, which leads to the inverse square root dependence in Eq. (35). Different particles present in non-Newtonian fluids (e.g. solids and polymer molecules) are deposited according to different laws, which makes a detailed modelling of the leak-off process a formidable challenge only partially resolved and only for some specific types of fluids, e.g. a water-based mud with a polymer in ref. (Lohne et al., 2010).

4. Discussion and conclusions

In addition to the issues specific for non-Newtonian fluids, there are some generic issues common to flow modelling of both Newtonian and non-Newtonian fluids. For instance, there is evidence that representative elementary volume exists neither for single fractures (Lavrov, 2021b; Méheust and Schmittbuhl, 2000) nor for fracture networks (Berre et al., 2019). This might challenge the utility of numerical flow modelling in fractured rock altogether.

Another challenge common to all types of network flow simulations and all types of fluids is the quality of fracture characterization. For instance, there is evidence suggesting that a correlation between fracture aperture and length may significantly affect the propagation of a non-Newtonian fluid displacing a Newtonian fluid in place (Zou et al., 2019). Therefore, meaningful prediction from numerical models can be made only if the fracture network has been characterized quantitatively in sufficient detail.

Another challenging issue in modelling non-Newtonian fluid flow in fracture networks appears when one or more of the fluids have a nonzero yield stress. When the pressure gradient in a given fracture is sufficiently small, the flow rate becomes zero, and the fracture needs effectively to be excluded from the model. Two common ways to deal with this issue are (i) by considering only the flow problems where every fracture flows, i.e. the pressure gradients are all above the zero-flow threshold or (b) by introducing a regularization into the rheological model so that there is always nonzero flow rate at arbitrary small pressure gradients (Zou et al., 2019). Approach (a) only works well when the injection pressure is sufficiently high to ensure flow in the entire connected network. Approach (b) can be used at arbitrarily small pressure gradients but creates a false impression that the entire network always flows. Developing an effective numerical algorithm that would solve the fracture exclusion problem caused by nonzero yield stress is an outstanding task.

The following challenges and knowledge gaps have been identified in the realm of non-Newtonian fluid flow in fractures and fracture networks:

- Effect of hardening and thixotropy on fracture flow, especially in cyclic flow regimes (cyclic injection, borehole ballooning), has not been properly addressed. Modelling of cement hardening is usually oversimplified in numerical models of grouting.
- The validity of the lubrication theory approximation for non-Newtonian fluid flow in rough-walled fractures has not been analyzed. The criteria for using/not using the lubrication theory are not established.
- It is not clear whether the three flow regimes (piston, fingering, bubble flow) experimentally observed in low-*Re* two-phase flows involving non-Newtonian fluids in Hele-Shaw cells are the only

regimes possible. Flow regimes at higher Reynolds numbers have not been studied.

- Quantitative criteria that would allow prediction of the flow regimes in two-phase fracture flow need to be established by means of experiments, numerical and analytical modelling in a wide range of rheological parameters and flow rates. Currently, this is largely an outstanding task.
- Effects of different flow regimes (high/low *Re*, pressure pulsations) on fluid displacement and grouting efficiency require clarification (Draganović and Stille, 2014).
- Flow of non-Newtonian fluids with leak-off through the fracture wall needs to be studied further (Zhang et al., 2019). This is important e.g. for hydraulic fracturing applications.
- Fracture opening/closing is usually assumed negligible in DFN models (Hässler et al., 1992), or is included in a very simplified way, e.g. by making the local fracture aperture a linear function of the local pressure (Dokhani et al., 2020; Lavrov and Tronvoll, 2004). While this assumption might be justified in some applications, its significance and validity should be properly investigated.
- Some non-Newtonian fluids are suspensions of solid particles in a carrier fluid. Flow of such fluids in fractures is additionally complicated by particle transport, settling and deposition as well as by dehydration of suspension due to leakoff through the fracture walls. In numerical modelling of suspension flows in fractures, it is usually assumed that there is no slip between the solids and the carrier fluid. This simplifies the solution substantially by effectively reducing the flow problem to single-phase (Adachi et al., 2007).
- A number of assumptions are commonly made when modelling single-phase flow in fractures and fracture networks. The flow is usually assumed to be incompressible non-inertial laminar isothermal. In some works, fluids are treated as compressible though (Liu et al., 2021).
- In multiphase flow, the flow is often, in addition, assumed to be miscible (zero interfacial tension) but miscibility is assumed negligible at the time scale of the problem in hand (Boronin et al., 2015).
- In DFN models, mixing laws for non-Newtonian and Newtonian fluids meeting at a fracture intersection should be derived from dedicated, detailed numerical modelling. Current practice is based on assuming some oversimplified phenomenological mixing rules. What really happens at an intersection, even in a two-dimensional DFN, is unclear.
- In today's engineering practice, non-Newtonian fluid flows in fractures often represent coupled multiphysics problems where several physical processes affect each other. An example is hydraulic fracturing, where a non-Newtonian fracturing fluid interacts with the deformable rock mass, contributes to the heat transfer, and deposits solids on the fracture walls. These processes, in turn, affect the fluid flow (Lavrov, 2017a). Numerical modelling of such coupled phenomena is still a challenge.

Author statement

A. Lavrov: Conceptualization; Formal analysis; Investigation; Methodology; Writing - original draft; Writing - revision.

Declaration of Competing Interest

The author declares that he has no known competing financial interests or personal relationships that could have appeared to influence the work reported in this paper.

Data availability

No data was used for the research described in the article.

References

Adachi, J., Siebrits, E., Peirce, A., Desroches, J., 2007. Computer simulation of hydraulic fractures. Int. J. Rock Mech. Min. Sci. 44, 739–757.

Aghajannezhad, P., Sellier, M., Becker, S., 2021. Patching Hele-Shaw cells to investigate the flow at low Reynolds number in fracture networks. Transp. Porous Media 136, 147–163. https://doi.org/10.1007/s11242-020-01505-x.

Amadei, B., Savage, W.Z., 2001. An analytical solution for transient flow of Bingham viscoplastic materials in rock fractures. Int. J. Rock Mech. Min. Sci. 38, 285–296.

Auradou, H., Boschan, A., Chertcoff, R., Gabbanelli, S., Hulin, J.P., Ippolito, I., 2008. Enhancement of velocity contrasts by shear-thinning solutions flowing in a rough fracture. J. Non-Newtonian Fluid Mech. 153, 53–61. https://doi.org/10.1016/j.jnnfm.2007.11.008.

Baik, M.-H., Cho, W.-J., Hahn, P.-S., 2007. Erosion of bentonite particles at the interface of a compacted bentonite and a fractured granite. Eng. Geol. 91, 229–239. https://doi.org/10.1016/j.enggeo.2007.02.002.

Bao, K., Lavrov, A., Nilsen, H.M., 2017. Numerical modeling of non-Newtonian fluid flow in fractures and porous media. Comput. Geosci. 21, 1313–1324.

Barbati, A.C., Desroches, J., Robisson, A., McKinley, G.H., 2016. Complex fluids and hydraulic fracturing. In: Annual Review of Chemical and Biomolecular Engineering, 7, pp. 415–453.

Barnes, H.A., Walters, K., 1985. The yield stress myth? Rheol. Acta 24, 323–326. https://doi.org/10.1007/BF01333960.

Békri, S., Thovert, J.F., Adler, P.M., 1997. Dissolution and deposition in fractures. Eng. Geol. 48, 283–308. https://doi.org/10.1016/S0013-7952(97)00044-6.

Berre, I., Doster, F., Keilegavlen, E., 2019. Flow in fractured porous media: a review of conceptual models and discretization approaches. Transp. Porous Media 130, 215–236.

Billingham, J., Ferguson, J.W.J., 1993. Laminar, unidirectional flow of a thixotropic fluid in a circular pipe. J. Non-Newtonian Fluid Mech. 47, 21–55. https://doi.org/10.1016/0377-0257(93)80043-B.

Boon, W.M., Nordbotten, J.M., Yotov, I., 2018. Robust discretization of flow in fractured porous media. SIAM J. Numer. Anal. 56, 2203–2233. https://doi.org/10.1137/17m1139102.

Boronin, S.A., Osiptsov, A.A., Desroches, J., 2015. Displacement of yield-stress fluids in a fracture. Int. J. Multiphase Flow 76, 47–63. https://doi.org/10.1016/j.ijmultiphaseflow.2015.07.001.

Brown, S.R., 1987. Fluid flow through rock joints: the effect of surface roughness. J. Geophys. Res. B 92, 1337–1347.

Brush, D.J., Thomson, N.R., 2003. Fluid flow in synthetic rough-walled fractures: Navier-Stokes, Stokes, and local cubic law simulations. Water Resour. Res. 39 https://doi.org/10.1029/2002WR001346.

Caenn, R., Darley, H.C.H., Gray, G.R., 2011. Composition and Properties of Drilling and Completion Fluids. Elsevier, Amsterdam.

Cayeux, E., 2020. Time, pressure and temperature dependent rheological properties of drilling fluids and their automatic measurements. In: SPE paper 199641 presented at the IADC/SPE International Drilling Conference and Exhibition.

Cayeux, E., Leulseged, A., 2019. Effect of solid particle concentration on drilling fluid rheological behavior and its impact on pressure losses. In: SPE paper 194131 presented at the SPE/IADC International Drilling Conference and Exhibition.

Cerasi, P., Ladva, H.K., Bradbury, A.J., Soga, K., 2001. Measurement of the mechanical properties of filtercakes. In: SPE Paper 68948. SPE European Formation Damage Conference.

Chhabra, R.P., Richardson, J.F., 1999. Non-Newtonian Flow in the Process Industries. Butterworth-Heinemann, Oxford.

Chin, W.C., 2012. Managed Pressure Drilling: Modeling. Strategy and Planning, Elsevier, Amsterdam.

Coussot, P., 1999. Saffman–Taylor instability in yield-stress fluids. J. Fluid Mech. 380, 363–376. https://doi.org/10.1017/S002211209800370X.

Dai, Z., Huang, Y., Cheng, H., Xu, Q., 2014. 3D numerical modeling using smoothed particle hydrodynamics of flow-like landslide propagation triggered by the 2008 Wenchuan earthquake. Eng. Geol. 180, 21–33. https://doi.org/10.1016/j.enggeo.2014.03.018.

de Dreuzy, J.-R., Davy, P., Bour, O., 2002. Hydraulic properties of two-dimensional random fracture networks following power law distributions of length and aperture. Water Resour. Res. 38 https://doi.org/10.1029/2001WR001009, 12-11-12-19.

Di Federico, V., 1997. Estimates of equivalent aperture for non-Newtonian flow in a rough-walled fracture. Int. J. Rock Mech. Min. Sci. 34, 1133–1137.

Dokhani, V., Ma, Y., Geng, T., Li, Z., Yu, M., 2020. Transient analysis of mud loss in fractured formations. J. Pet. Sci. Eng. 195, 107722 https://doi.org/10.1016/j.petrol.2020.107722.

Draganović, A., Stille, H., 2014. Filtration of cement-based grouts measured using a long slot. Tunn. Undergr. Space Technol. 43, 101–112. https://doi.org/10.1016/j.tust.2014.04.010.

Eriksson, M., Stille, H., Andersson, J., 2000. Numerical calculations for prediction of grout spread with account for filtration and varying aperture. Tunn. Undergr. Space Technol. 15, 353–364. https://doi.org/10.1016/S0886-7798(01)00004-9.

Fidelibus, C., Lenti, V., 2012. The propagation of grout in pipe networks. Comput. Geosci. 45, 331–336.

Foroushan, H.K., Ozbayoglu, E.M., Miska, S.Z., Yu, M., Gomes, P.J., 2018. On the instability of the cement/fluid interface and fluid mixing. SPE Drill. Complet. 33, 63–76. https://doi.org/10.2118/180322-pa.

Freitas, J.F., Soares, E.J., Thompson, R.L., 2013. Viscoplastic–viscoplastic displacement in a plane channel with interfacial tension effects. Chem. Eng. Sci. 91, 54–64. https://doi.org/10.1016/j.ces.2013.01.031.

Frigaard, I.A., Nouar, C., 2005. On the usage of viscosity regularisation methods for visco-plastic fluid flow computation. J. Non-Newtonian Fluid Mech. 127, 1–26. https://doi.org/10.1016/j.jnnfm.2005.01.003.

Funehag, J., Thörn, J., 2018. Radial penetration of cementitious grout – Laboratory verification of grout spread in a fracture model. Tunn. Undergr. Space Technol. 72, 228–232. https://doi.org/10.1016/j.tust.2017.11.020.

Grindrod, P., Peletier, M., Takase, H., 1999. Mechanical interaction between swelling compacted clay and fractured rock, and the leaching of clay colloids. Eng. Geol. 54, 159–165. https://doi.org/10.1016/S0013-7952(99)00071-X.

Gustafson, G., Stille, H., 1996. Prediction of groutability from grout properties and hydrogeological data. Tunn. Undergr. Space Technol. 11, 325–332. https://doi.org/10.1016/0886-7798(96)00027-2.

Hallot, E., Davy, P., de Bremond d'Ars, J., Auvray, B., Martin, H., Van Damme, H., 1996. Non-Newtonian effects during injection in partially crystallised magmas. J. Volcanol. Geotherm. Res. 71, 31–44. https://doi.org/10.1016/0377-0273(95)00061-5.

Hanssen, A., 2013. Numerical Modelling of Bingham Fluid Flow and Particle Transport in a Rough-Walled Fracture. MSc. Norges teknisk-naturvitenskapelige universitet (NTNU).

Hässler, L., Håkansson, U., Stille, H., 1992. Computer-simulated flow of grouts in jointed rock. Tunn. Undergr. Space Technol. 7, 441–446.

Hatheway, A.W., Reeves, G.M., 1999. A second review of the international status of engineering geology — encompassing hydrogeology, environmental geology and the applied geosciences. Eng. Geol. 53, 259–296. https://doi.org/10.1016/S0013-7952(99)00046-0.

Hyman, J.D., Jiménez-Martínez, J., Viswanathan, H.S., Carey, J.W., Porter, M.L., Rougier, E., Karra, S., Kang, Q., Frash, L., Chen, L., Lei, Z., O'Malley, D., Makedonska, N., 2016. Understanding hydraulic fracturing: a multi-scale problem. Philos. Trans. R. Soc. A Math. Phys. Eng. Sci. 374, 20150426. https://doi.org/10.1098/rsta.2015.0426.

Irgens, F., 2008. Continuum Mechanics. Springer.

Kondic, L., Shelley, M.J., Palffy-Muhoray, P., 1998. Non-Newtonian Hele-Shaw flow and the Saffman-Taylor instability. Phys. Rev. Lett. 80, 1433–1436. https://doi.org/10.1103/PhysRevLett.80.1433.

Koponen, A., Kataja, M., Timonen, J., 1996. Tortuous flow in porous media. Phys. Rev. E 54, 406–410. https://doi.org/10.1103/PhysRevE.54.406.

Koyama, T., Fardin, N., Jing, L., Stephansson, O., 2006. Numerical simulation of shear-induced flow anisotropy and scale-dependent aperture and transmissivity evolution of rock fracture replicas. Int. J. Rock Mech. Min. Sci. 43, 89–106. https://doi.org/10.1016/j.ijrmms.2005.04.006.

Lakhtychkin, A., Eskin, D., Vinogradov, O., 2012. Modelling of transport of two proppant-laden immiscible power-law fluids through an expanding fracture. Can. J. Chem. Eng. 90, 528–543. https://doi.org/10.1002/cjce.20694.

Lavrov, A., 2005. Modeling flow of a biviscous fluid from borehole into rock fracture. ASME J. Appl. Mech. 73, 171–173.

Lavrov, A., 2013a. Numerical modeling of steady-state flow of a non-Newtonian power-law fluid in a rough-walled fracture. Comput. Geotech. 50, 101–109. https://doi.org/10.1016/j.compgeo.2013.01.004.

Lavrov, A., 2013b. Redirection and channelization of power-law fluid flow in a rough-walled fracture. Chem. Eng. Sci. 99, 81–88. https://doi.org/10.1016/j.ces.2013.05.045.

Lavrov, A., 2015. Flow of truncated power-law fluid between parallel walls for hydraulic fracturing applications. J. Non-Newtonian Fluid Mech. 223, 141–146. https://doi.org/10.1016/j.jnnfm.2015.06.005.

Lavrov, A., 2016. Lost Circulation: Mechanisms and Solutions. Elsevier, Oxford.

Lavrov, A., 2017a. Chapter 3 - Coupling in hydraulic fracturing simulation. In: Porous Rock Fracture Mechanics. Elsevier / Woodhead Publishing, pp. 47–62.

Lavrov, A., 2017b. Lost circulation in primary well cementing. Energy Procedia 114, 5182–5192. https://doi.org/10.1016/j.egypro.2017.03.1672.

Lavrov, A., 2021a. Fluid displacement in a 2D DFN fracture: time integration of the interface position. Transp. Porous Media 139, 247–269. https://doi.org/10.1007/s11242-021-01659-2.

Lavrov, A., 2021b. Million node fracture: size matters? J. Pet. Explor. Prod. Technol. 11, 4269–4276. https://doi.org/10.1007/s13202-021-01296-x.

Lavrov, A., 2022. Robertson-Stiff rheological model in fracture flow. J. Pet. Sci. Eng. 217, 110935 https://doi.org/10.1016/j.petrol.2022.110935.

Lavrov, A., Laux, H., 2007. DEM modeling of particle restitution coefficient vs Stokes number: The role of lubrication force. Paper No S2_Thu_C_54. In: 6th International Conference on Multiphase Flow, ICMF 2007, Leipzig, Germany, July 9–13, 2007.

Lavrov, A., Tronvoll, J., 2004. Modeling mud loss in fractured formations. In: SPE paper 88700 presented at the 11th Abu Dhabi International Petroleum Exhibition and Conference held in Abu Dhabi, U.a.E., 10-13 October 2004.

Lavrov, A., Tronvoll, J., 2005. Mechanics of borehole ballooning in naturally-fractured formations. In: SPE Paper 93747. SPE Middle East Oil and Gas Show and Conference.

Lei, Q., Latham, J.-P., Tsang, C.-F., 2017. The use of discrete fracture networks for modelling coupled geomechanical and hydrological behaviour of fractured rocks. Comput. Geotech. 85, 151–176.

Lejeune, A.-M., Richet, P., 1995. Rheology of crystal-bearing silicate melts: an experimental study at high viscosities. J. Geophys. Res. Solid Earth 100, 4215–4229. https://doi.org/10.1029/94JB02985.

Lenci, A., Chiapponi, L., 2020. An experimental setup to investigate non-Newtonian fluid flow in variable aperture channels. Water 12.

Lenci, A., Di Federico, V., 2020. A channel model for bi-viscous fluid flow in fractures. Transp. Porous Media 134, 97–116.

Lenci, A., Méheust, Y., Putti, M., Di Federico, V., 2022a. Monte Carlo simulations of shear-thinning flow in geological fractures. Water Resour. Res. 58 https://doi.org/10.1029/2022WR032024 e2022WR032024.

Lenci, A., Putti, M., Di Federico, V., Méheust, Y., 2022b. A lubrication-based solver for shear-thinning flow in rough fractures. Water Resour. Res. 58 https://doi.org/10.1029/2021WR031760 e2021WR031760.

Lindner, A., Bonn, D., PoirÉ, E.C., Amar, M.B., Meunier, J., 2002. Viscous fingering in non-Newtonian fluids. J. Fluid Mech. 469, 237–256. https://doi.org/10.1017/S0022112002001714.

Liu, Q., Lei, G., Peng, X., Lu, C., Wei, L., 2018. Rheological characteristics of cement grout and its effect on mechanical properties of a rock fracture. Rock Mech. Rock. Eng. 51, 613–625. https://doi.org/10.1007/s00603-017-1340-x.

Liu, X., Hu, C., Liu, Q., He, J., 2021. Grout penetration process simulation and grouting parameters analysis in fractured rock mass using numerical manifold method. Eng. Analys. Bound. Elem. 123, 93–106. https://doi.org/10.1016/j.enganabound.2020.11.008.

Lohne, A., Han, L., van der Zwaag, C., van Velzen, H., Mathisen, A.-M., Twynam, A., Hendriks, W., Bulgachev, R., Hatzignatiou, D.G., 2010. Formation-damage and well-productivity simulation. SPE J. 15, 751–769. https://doi.org/10.2118/122241-pa.

Ma, W., Tomac, I., 2021. Experimental investigation of proppant clustering in intersected fractures. J. Petroleum Explorat. Product. 11, 1727–1742. https://doi.org/10.1007/s13202-021-01122-4.

Ma, G.W., Wang, H.D., Fan, L.F., Wang, B., 2017. Simulation of two-phase flow in horizontal fracture networks with numerical manifold method. Adv. Water Resour. 108, 293–309.

Ma, G.W., Wang, H.D., Fan, L.F., Chen, Y., 2018. Segmented two-phase flow analysis in fractured geological medium based on the numerical manifold method. Adv. Water Resour. 121, 112–129.

Majidi, R., Miska, S.Z., Thompson, L.G., Yu, M., 2008. Quantitative analysis of mud losses in naturally fractured reservoirs: the effect of rheology. In: SPE paper 114130 Presented at the SPE Western Regional and Pacific Section AAPG Joint Meeting.

Majidi, R., Miska, S.Z., Ahmed, R., Yu, M., Thompson, L.G., 2010a. Radial flow of yield-power-law fluids: Numerical analysis, experimental study and the application for drilling fluid losses in fractured formations. J. Pet. Sci. Eng. 70, 334–343. https://doi.org/10.1016/j.petrol.2009.12.005.

Majidi, R., Miska, S.Z.Z., Yu, M., Thompson, L.G.G., Zhang, J., 2010b. Quantitative analysis of mud losses in naturally fractured reservoirs: the effect of rheology. SPE Drill. Complet. 25, 509–517. https://doi.org/10.2118/114130-pa.

Martin, V., Jaffré, J., Roberts, J.E., 2005. Modeling fractures and barriers as interfaces for flow in porous media. SIAM J. Sci. Comput. 26, 1667–1691. https://doi.org/10.1137/s1064827503429363.

Méheust, Y., Schmittbuhl, J., 2000. Flow enhancement of a rough fracture. Geophys. Res. Lett. 27, 2989–2992. https://doi.org/10.1029/1999GL008464.

Mehr, N., Roques, C., Méheust, Y., Rochefort, S., Selker, J.S., 2020. Mixing and finger morphologies in miscible non-Newtonian solution displacement. Exp. Fluids 61, 96. https://doi.org/10.1007/s00348-020-2932-x.

Metwally, M., Nguyen, T., Wiggins, H., Saasen, A., Gipson, M., 2022. Experimental lab approach for water based drilling fluid using polyacrylamide friction reducers to drill extended horizontal wells. J. Pet. Sci. Eng. 110132 https://doi.org/10.1016/j.petrol.2022.110132.

Mohajerani, S., Baghbanan, A., Bagherpour, R., Hashemolhosseini, H., 2015. Grout penetration in fractured rock mass using a new developed explicit algorithm. Int. J. Rock Mech. Min. Sci. 80, 412–417. https://doi.org/10.1016/j.ijrmms.2015.06.013.

Morris, J.P., Chochua, G.G., Bogdan, A.V., 2015. An efficient non-newtonian fluid-flow simulator for variable aperture fractures. Can. J. Chem. Eng. 93, 1902–1915. https://doi.org/10.1002/cjce.22314.

O'Donovan, E.J., Tanner, R.I., 1984. Numerical study of the Bingham squeeze film problem. J. Non-Newtonian Fluid Mech. 15, 75–83. https://doi.org/10.1016/0377-0257(84)80029-4.

Ofei, T.N., Lund, B., Saasen, A., 2021. Effect of particle number density on rheological properties and barite sag in oil-based drilling fluids. J. Pet. Sci. Eng. 206, 108908 https://doi.org/10.1016/j.petrol.2021.108908.Öge, İ.F., 2017. Prediction of cementitious grout take for a mine shaft permeation by adaptive neuro-fuzzy inference system and multiple regression. Eng. Geol. 228, 238–248. https://doi.org/10.1016/j.enggeo.2017.08.013.

Papanastasiou, T.C., 1987. Flows of materials with yield. J. Rheol. 31, 385–404.

Pascal, H., 1984. Rheological behaviour effect of non-newtonian fluids on dynamic of moving interface in porous media. Int. J. Eng. Sci. 22, 227–241. https://doi.org/10.1016/0020-7225(84)90003-X.

Perkowska, M., Wrobel, M., Mishuris, G., 2016. Universal hydrofracturing algorithm for shear-thinning fluids: Particle velocity based simulation. Comput. Geotech. 71, 310–337. https://doi.org/10.1016/j.compgeo.2015.10.005.

Ralston, A., Rabinowitz, P., 2016. A First Course in Numerical Analysis, 2nd edition. Dover Publications.

Ren, J., Deshun, Y., Zhai, R., 2021. Rheological behavior of bentonite-water suspension at various temperatures: effect of solution salinity. Eng. Geol. 295, 106435 https://doi.org/10.1016/j.enggeo.2021.106435.

Rodríguez de Castro, A., Radilla, G., 2017. Flow of yield stress and Carreau fluids through rough-walled rock fractures: Prediction and experiments. Water Resour. Res. 53, 6197–6217. https://doi.org/10.1002/2017WR020520.

Rossen, W.R., Kumar, A.T.A., 1992. Single- and two-phase flow in natural fractures. In: SPE paper 24915 presented at the 67th Annual Technical Conference and Exhibition.

Russian, A., Riva, M., Russo, E.R., Chiaramonte, M.A., Guadagnini, A., 2019. Stochastic inverse modeling and global sensitivity analysis to assist interpretation of drilling mud losses in fractured formations. Stoch. Env. Res. Risk A. 33, 1681–1697. https://doi.org/10.1007/s00477-019-01729-4.

Ryerson, F.J., Weed, H.C., Piwinskii, A.J., 1988. Rheology of subliquidus magmas: 1. Picritic compositions. J. Geophys. Res. Solid Earth 93, 3421–3436. https://doi.org/10.1029/JB093iB04p03421.

Saffman, P.G., Taylor, G.I., 1958. The penetration of a fluid into a porous medium or Hele-Shaw cell containing a more viscous liquid. Proceed. Royal Soc. London. Series A. Math. Phys. Sci. 245, 312–329. https://doi.org/10.1098/rspa.1958.0085.

Sayindla, S., Lund, B., Ytrehus, J.D., Saasen, A., 2019. CFD modeling of hydraulic behavior of oil- and water-based drilling fluids in laminar flow. SPE Drill. Complet. 34, 207–215. https://doi.org/10.2118/184660-pa.

Selvadurai, A.P.S., Nguyen, T.S., 1999. Mechanics and fluid transport in a degradable discontinuity. Eng. Geol. 53, 243–249. https://doi.org/10.1016/S0013-7952(99)00040-X.

Seright, R.S., 2001. Gel propagation through fractures. SPE Product. Facilit. 16, 225–231. https://doi.org/10.2118/74602-pa.

Taheri, A., Ytrehus, J.D., Lund, B., Torsæter, M., 2021. Use of concentric Hele-Shaw cell for the study of displacement flow and interface tracking in primary cementing. Energies 14, 51.

Tomac, I., Gutierrez, M., 2015. Micromechanics of proppant agglomeration during settling in hydraulic fractures. J. Pet. Explor. Prod. Technol. 5, 417–434. https://doi.org/10.1007/s13202-014-0151-9.

Tomac, I., Tartakovsky, D.M., 2018. Experimental evaluation of turbulent flow and proppant ytansport in a narrow fracture. In: Proceedings of the 43rd Workshop on Geothermal Reservoir Engineering. Stanford University, Stanford, California. February 12–14, 2018.

Unsal, E., Matthäi, S.K., Blunt, M.J., 2010. Simulation of multiphase flow in fractured reservoirs using a fracture-only model with transfer functions. Comput. Geosci. 14, 527–538. https://doi.org/10.1007/s10596-009-9168-4.

Valkó, P., Economides, M.J., 1995. Hydraulic Fracture Mechanics. Wiley, Chichester.

Wang, Z., Xu, C., Dowd, P., 2018. A Modified Cubic Law for single-phase saturated laminar flow in rough rock fractures. Int. J. Rock Mech. Min. Sci. 103, 107–115. https://doi.org/10.1016/j.ijrmms.2017.12.002.

Wrobel, M., 2020. An efficient algorithm of solution for the flow of generalized Newtonian fluid in channels of simple geometries. Rheol. Acta 59, 651–663.

Wrobel, M., Mishuris, G., 2015. Hydraulic fracture revisited: Particle velocity based simulation. Int. J. Eng. Sci. 94, 23–58. https://doi.org/10.1016/j.ijengsci.2015.04.003.

Wrobel, M., Mishuris, G., Papanastasiou, P., 2021. On the influence of fluid rheology on hydraulic fracture. Int. J. Eng. Sci. 158, 103426 https://doi.org/10.1016/j.ijengsci.2020.103426.

Wüst, R.A.J., McLane, J., 2000. Rock deterioration in the Royal Tomb of Seti I, Valley of the Kings, Luxor, Egypt. Eng. Geol. 58, 163–190. https://doi.org/10.1016/S0013-7952(00)00057-0.

Yoon, J., El Mohtar, C.S., 2014. Rheological properties of sodium pyrophosphate modified bentonite suspensions for seepage control. Eng. Geol. 179, 32–40. https://doi.org/10.1016/j.enggeo.2014.06.012.

Zhang, M., Prodanović, M., Mirabolghasemi, M., Zhao, J., 2019. 3D microscale flow simulation of shear-thinning fluids in a rough fracture. Transp. Porous Media 128, 243–269. https://doi.org/10.1007/s11242-019-01243-9.

Zimmerman, R.W., Kumar, S., Bodvarsson, G.S., 1991. Lubrication theory analysis of the permeability of rough-walled fractures. Int. J. Rock Mech. Min. Sci. Geomech. Abstr. 28, 325–331. https://doi.org/10.1016/0148-9062(91)90597-F.

Zou, L., Jing, L., Cvetkovic, V., 2017. Modeling of flow and mixing in 3D rough-walled rock fracture intersections. Adv. Water Resour. 107, 1–9. https://doi.org/10.1016/j.advwatres.2017.06.003.

Zou, L., Håkansson, U., Cvetkovic, V., 2018. Two-phase cement grout propagation in homogeneous water-saturated rock fractures. Int. J. Rock Mech. Min. Sci. 106, 243–249.

Zou, L., Håkansson, U., Cvetkovic, V., 2019. Cement grout propagation in two-dimensional fracture networks: Impact of structure and hydraulic variability. Int. J. Rock Mech. Min. Sci. 115, 1–10. https://doi.org/10.1016/j.ijrmms.2019.01.004.

Zou, L., Håkansson, U., Cvetkovic, V., 2020. Yield-power-law fluid propagation in water-saturated fracture networks with application to rock grouting. Tunn. Undergr. Space Technol. 95, 103170 https://doi.org/10.1016/j.tust.2019.103170.